An Earthquake Source Model with a Ripple Generating Core(Dissertation_全文)

AUTHOR(S):

Umeda, Yasuhiro

CITATION:

Umeda, Yasuhiro. An Earthquake Source Model with a Ripple Generating Core. 京都大学, 1982, 理学博士

ISSUE DATE:

1982-03-23

URL:

https://doi.org/10.14989/doctor.r4641

学位申請論文

梅田康弘

論 文 内 容 の 要 旨

報告番号	乙第　　号	氏名	梅田康弘
論文調査担当者	主査　三雲　健 三木晴男　岸本兆方		

（論文題目）

An Earthquake Source Model with a Ripple Generating Core

（リプル発生核をもつ震源モデル）

（論文内容の要旨）

一般に観測される地震波には震源の破壊による影響や、震源付近の地殻構造、途中の伝播経路の構造、観測点付近の構造などの影響が含まれ、かなり複雑である。

申請者が行なった研究は、広帯域の地震計記録、主として阿武山地震観測所の大震計及び強震計によって比較的近距離で観測された地震記録をもとに、さらに余震分布、震源付近での地震時の水平変位分布、震度分布などの過去のデータをあわせ考慮して、マグニチュードが7を超えるいくつかの浅発大地震の破壊過程を追究しようとしたものである。こゝで対象とした4個の大地震の際に長周期地震波に重畳して観測された短周期地震波（こゝではこの波のことをリプルと呼ぶ）は、1）長周期波に重なってはいるが、周波数領域では完全に分離して大きい振幅のピークを持ち、かつ2）P波とS波それぞれの初動部分の短かい時間に出現することが明らか

となった。申請者はこのような特徴が、主断層上で滑らかなdislocationが始まった直後の限られた短かい時間内に、多数の小破壊が比較的狭い領域で発生したと考え、この領域のことを"リプル発生核"と呼んだ。このような推測を確めるために申請者は震源近傍で観測された過去のデータを検討した結果、1）本震発生直後の余震活動は上の領域内で特に低いこと、2）この領域周辺では、測地学的、地質学的に推定される地震時の静的断層変位が特に大きいこと、3）家屋の倒壊率などから推定される震度線がこの領域付近に集中していること、4）この領域の拡がりは主断層の長さに比べてかなり小さいこと等の顕著な事実があることを見出した。

以上のような観測結果から、申請者はリプルを発生する領域を持つような震源モデルを提出し、この領域の中では主断層に平行な多数の小断層が主破壊の開始直後に一定の時間間隔で次々とずりを起すことによって短周期地震波を発生させると仮定して、これら小断層の大きさ、変位や時間間隔の推定を試みた。小断層の大きさとずり変位(d)はスケール則を仮定して短周期波と長周期波の周期比から推定し、破壊進行速度(v)とライズタイム(τ)は $v \leq \beta$、$d/2\tau < \beta\varepsilon$（$\beta$：S波速度、$\varepsilon$：限界歪）の条件から仮定し、小断層破壊の時間間隔は合成地震記象と観測記録の比較から想定した。この結果、こゝで対象としたM＞7の大地震の発生過程がこのような震源モデルで説明されることを主張している。

主論文

An Earthquake Source Model With a Ripple Generating Core

Yasuhiro UMEDA

Abuyama Seismological Observatory, Faculty of Science,
Kyoto University, Takatsuki, Japan

CONTENTS

Abstract

The rupture processes of large shallow earthquakes are investigated based on the broad-band seismograms recorded at relatively short focal distances as well as on various field surveys near the source regions. Predominant short-period waves are recorded only during a short period at the initial parts of P- and S-waves. These waves give a prominent spectral peak at high frequencies. The results from coseismic and postseismic field surveys in some source regions clearly show that there must be a particular region characterized by a large dislocation, large acceleration and extremely low aftershock activity. This specific region seems to have a relatively small dimension compared with the length of the main fault.

A source model is proposed so as to satisfy various aspects of the observed results. In this model, the rupture processes in a source region may be divided into two stages. The first stage is the smoothing dislocation propagating over the main fault and the second one is the complex ruptures of many small faults distributed in a confined small region. The long-period waves are produced by the former stage. The latter stage radiates the predominant short-period waves, yielding a spectral peak at high frequencies. It is assumed that a large number of small faults with the same fault geometry and the same fault motion are arranged en echelon or parallel in this specific region, and that these small elements are dislocated simultaneously and successibly in a short time after the onset of main rupture. We call this specific region in the earthquake source area " a ripple generating core ".

The stress drop by each small fault may be of the same order

as that of the main fault, if static and dynamic fault parameters are estimated on the basis of the earthquake scaling law. Extremely low activity of aftershocks within the specific region may be caused by the distribution of many small ruptures. A large amount of dislocation around this specific region appear to arise from the accumulation of these abundant dislocations.

1. Introduction

Long-period seismic waves have been well explained by a simple uniform dislocation model, whereas short-period waves observed at short focal distances are scarcely explained by this simple model. Increased attention has recently been paid to explain these predominant short-period waves.

HARTZELL and BRUNE(1979) suggested two-stage stress release processes based on the study of the Horse Canyon earthquake of Aug.2,1975. Although their model well explained the difference in the seismic moments obtained by short-period body waves and long-period surface waves, the duration of short-period waves have not satisfactorily been explained. DAS and AKI(1977) introduced a fault plane with barriers as a versatile earthquake model, and clearly explained "ripples" involved in seismograms. The abnormal departure from a scaling law of the seismic spectrum was also explained by this model. MIKUMO and MIYATAKE(1978) have proposed a fault model consisting of many high strength areas distributed over a fault surface, and explained the duration of short-period waves and the seismic spectrum observed at a relatively short focal distance.

In this paper we are concerned with the broad band characteristics of seismic waves. At the Abuyama Seismological Observatory, the broad-band and wide-dynamic range seismograph system has been installed, and a number of remarkable earthquakes at relatively short focal distances have been well recorded. With these seismograms it is possible to gain further information on the rupture process in the focal region. Especially the predominant short-period waves provide us a finer understanding of this process than the long-period waves.

It is important for a proposed fault model to explain not only seismograms but coseismic static and dynamic field phenomena. Such field observations, however, are available only under very favarable circumstances. Earthquakes must be large enough to reflect the above various effects on the earth's surface. Further, to make a comprehensive survey of these phenomena, they have to occur on land. For a few earthquakes which have recently occurred in Japan, we will investigate coseismic crustal deformations, distributions of intensity and activities of aftershocks immediately after main shocks. Based on these results, a new source model will be introduced in this paper.

2. The Origin of Short-Period Waves

2.1 Broad-Band Seismograms

It is widely accepted that long-period seismic waves represent the gross features of the faulting process, and that the more detailed rupture process might be well reflected in short-period waves. In order to obtain detailed information on the earthquake sources, we have to investigate broad-band seismograms covering long-periods to short-periods. At the same time, it is necessary for us to record large earthquakes at short focal distances, because seismic waves recorded at long distances are more seriously affected by anelasticity and lateral heterogeneity of the earth.

The broad-band seismograph system at the Abuyama Seismological Observatory consists of long-period(T_o=24～27sec), low-magnification(V=1.1), and strong-motion type(T_o=1.4～6sec, V=5 or 15)seismometers. Their response curves are shown in Fig.1. The long-period seismographs with a recording stroke of about 30cm, may have a somewhat limited response to high frequencies of several heltz, due to their long pendulum arm(1.7m), in addition to a solid friction of 1mm. The seismograms are recorded on smoked paper. These instruments were devised by SASSA(SASSA,1941), which have been colloquially called "Sassa-type seismographs".

Epicenters of the events which have been made available through the recordings of the broad-band seismograph system are plotted in Fig.2, and some typical seismograms are shown in Figs. 3,5 and 6. The short-period waves discussed here are often recorded densely on the chart of low-magnification long-period seismograms. Some of the strong motion seismograms are scratched or smeared because of extremely short-periods and large amplitudes.

These predominant short-period waves are marked by τ_s only in the main part of S-waves. It should be noticed that these waves are also found at the early stages of P-waves, as clearly seen in the trace of strong motion in Fig.6.

2.2 Period and Duration of Short-Period Waves

In this section, the characteristics of short-period waves which may represent a detailed rupture process are mainly investigated in reference to those of long-period waves.

In the case of the Tottori earthquake(1943), the representative long-period wave has a period of about 15sec as seen in the two components of long-period seismograms(Fig.3), and this period is supposed to result from the rupture of a main fault with dimensions of 33 X 13km, a dislocation of 2.5m and an average rise time of 3sec(KANAMORI, 1972). On the contrary, the short-period waves overlapped on the long-period seismograms have often been ignored, because of indistinction or because the seismometers may not have responded enough to record the short-period as mentioned in the preceding section. However, as clearly seen on the strong-motion seismograms, these short-period waves with the periods of 0.4 or so are very predominant. The periods of these predominant short-period waves are about one fourtieth of those of the long-period waves. Although the main parts of the predominant waves are clipped, their amplitudes reach to half of those of the long-period waves.

It is noticed that the durations of these short-period waves do not continue from initial to coda of seismograms, but terminate in a short time(τ_s). This fact suggests that the rupture processes radiating these predominant short-period waves are terminated in a relatively short time.

The Fukui earthquake(1948) represents a multiple shock(Fig.5) which may be due to two successive large ruptures on the faults, as will be discussed in section 3.5. As is clearly seen on the E-W component of the long-period seismogram, the short-period waves with large amplitudes are found only on the first shock and not on the second. The separation of long-period and short-period waves is also remarkable. Further, these short-period waves are concentrated within a short time in an early part of P- and S-waves durations.

The period range of the Echizenmisaki-Oki earthquake(1963) migh have been sufficiently covered by the strong-motion seismometers with a natural period of 6sec at that time. The characteristics of short-period waves, as mentioned above, can be identified on a strong-motion seismogram(Fig.6). These features of short-period seismic waves are generally seen on the broad-band seismograms recorded at short focal distances for large shallow earthquakes.

2.3 Spectral Peak at High Frequencies

The broad-band spectra of seismic waves can be obtained by the procedure we undertook. The original seismograms were traced manually and transcribed onto an analogue magnetic tape by using a potentiometer. The long-period and strong-motion seismograms, stored in magnetic tape, were transformed into the frequency

domains by the FFT method. The respective output signals were corrected for the instrumental response to obtain the spectra of ground displacements. Then, a pair of spectra were added in the frequency domain. The broad-band seismic spectra thus obtained are shown in Fig.4 and 6.

We can find some noteworthy features in these spectra. The spectrum has a peak at a higher frequency range(2～5Hz), where the peak amplitude is 20～50 times larger than that inferred from a smoothing dislocation model(compare the seismic amplitudes with the broken lines in Figs.4 and 6). The large amplitudes at high frequency ranges implie the superposition of wavelets radiated from many small ruptures, because the amplitude of wavelets radiated from only one small rupture is too small to explain the peak level of the observed amplitude. These procedures will be discussed quantitatively in section 4.1. The spectral trough around 1Hz strongly indicates that the rupture dimensions do not vary continuously from large to small size. There might be a typical fault size corresponding to the peak frequency.

2.4 Error Estimation in Observed Waves and Calculated Spectra

Since short-period waves are affected by the crustal structure and the basement structure under the recording station, we will estimate these effects on the recorded seismic amplitudes and their errors on seismic spectra.

The velocity structure of the crust and the underground basement beneath the Abuyama Seismological Observatory have been investigated by artificial explosions(e.g.YOSHII et.al.,1974,

ITO and MURAKAMI,1978) and boring(OKANO and UMEDA,1974). The elementary basement structure is a paleozoic system. The crustal responses have been calculated for the plane P-waves with incidence angle of 90° (KANAI,1975). The results are shown in Fig.7 with layer thickness, velocity and assumed density. The amplitudes of short-period waves(0.2～0.5sec) amplified by the crustal layers are only a few times larger than those of long-period waves.

Error factor on the seismic spectra is also caused by the manual tracing of the original seismograms as described in the previous section. The results of some experiments show that the difficulty in tracing these short-periods is quite noticeable. A loss of 8db～2db is estimated at the period of 0.2～0.5sec.

The amplifications caused by the crustal structure and the basement structure should be taken into account on the observed seismograms. Both the amplification and the loss by manual tracing affect the seismic spectra calculations. The errors estimated above are, however, small in comparison with the observed short-period amplitudes, which are 20～50 times(26db～34db) larger than those expected from a smoothing dislocation over a single main fault.

2.5 Seismograms at Other Stations

Fortunately, certain features of short-period waves are confirmed by many seismological stations, but this is not the case with broad-band seismograms as described in section 2.1. A number of strong-motion seismographs(T_0=5 or 6sec, V=1) supported by the Japan Meteorological Agency have recorded many large earthquakes at relatively short focal distances. Some representative seismograms for two earthquakes are shown in Figs.8a

and 8b.

Although the lack of low-magnification and long-period seismograms restricts a comparison with long-period waves, predonimant short-period waves included in S-waves are clearly identified on these seismograms. The seismograms discussed here are sometimes smeared out because of extremely short-periods and large amplitudes, but we can confirm the following features by the aid of examinations in sections 2.1 and 2.2. The predominant short-period waves are concentrated within a short time(τ_s) in an early part of S-wave duration, and thus they may be distinguished from the relatively long-period duration time(τ_L). The relationships between these duration time and earthquake magnitudes are summarized in Fig.9.

Although the values scatter to some extent, presumably because of azimuthal irregularities, τ_s is nearly a third of τ_L. This fact supports the result in section 2.2, that is, the ruptures radiating predominant short-period waves terminate in a relatively short time.

2.6 The Conception of a Ripple Generating Core

The results derived from the seismic waves and their spectra lead to a postulation of the following rupture processes in the source area. Long-period and short-period waves are radiated from a smoothed rupture process over a main fault and from ruptures of many small elements, respectively. The observed large amplitudes of short-period waves are probably caused by the superpositions of wavelets radiated from a large number of small ruptures. And their ripples overling seismograms and a spectral peak at a higher frequency range suggest that the

rupture of many small elements occur successively.

It should be emphasized that the predominant short-period waves are concentrated in a relatively short time. This fact suggests that the rupture elements with small dimension are not distributed over the entire surface of a single main fault, but are concentrated in a relatively small region. Thus, there must be a specific region characterized by generation of the predominant short-period waves. In the following, the auther calls this specific region " a ripple generating core ". These conceptions are schematically shown in Fig.10.

In a field investigations, we can often find adjacent many small fault aligned in parallel or en echelon(e.g. MIZUTANI and KANAORI(1976), McGARR,at.al.(1979)). These actual observations support our postulations on the ripple generating core, that is, many faults are formed in a limited region.

3. Surface Phenomena of the Source Region

3.1 Expected Phenomena on the Earth's Surface

In order to seek other evidences which may be related to a ripple generating core, we shall here investigate surface phenomena around source region. Firstly, the activity of aftershocks immediately after the main shock occurrence may be affected by many small ruptures within the ripple generating core. Secondly, if the short-period waves are mainly radiated from this specific region, the isoseismals may have a center in this region. Thirdly, if many faults having the same fault motion and the same geometory are superposed in the region concerned, the total dislocation around the specific region will be quite large in comparison with the average dislocation along other portions of the main fault.

We will investigate some large shallow earthquakes with magnitudes greater than 7 since 1927. Aftershock locations have been remarkably well determined since the Tango earthquake of 1927, because of adopting mobile and temporary observation systems. For the earthquakes discussed in the following sections, fault parameters of the main fault have been obtained on the basis of the simple uniform dislocation model by a number of seismologists. A common features for these earthquakes is that they have nearly pure strike slips caused by a single stress system, i.e. east-west or north-south compression.

3.2 The Tango Earthquake of March 7, 1927(M=7.5)

Mobile observations of aftershock locations were carried out

by NASU(1929a, 1929b). The distribution of aftershocks within the first six days, from the paper by NASU(1935), is shown in Fig.11-A. It should be noticed that the aftershock activity was extremely low in the elliptical area surrounded by the broken line.

The coseismic static deformations resulting from this earthquake are shown in Figs.11-C and 11-D. Contours of equal maximum shear strains in this figure were obtained from the displacement data of triangulation points by TSUBOI(1932a). The dislocations along the fault were surveyed by NAKAMURA(1928), YAMASAKI and TADA(1928), WATANABE and SATO(1928) and recently compiled by MATSUDA(1976). The solid straight line in Figs.11-A, 11-B, 11-C shows the assumed fault with a length of 35km which has been estimated from seismic and geodetic data by KANAMORI(1973). The maximum shear strain and the total dislocations projected on the earth's surface are not uniform along the assumed fault, but they are especially large in the region surrounded by a broken line in Fig.11-C and indicated by a dotted line in Fig.11-D.

It is noticed that the area characterized by a large amount of dislocations coincides with the low active region of aftershocks. It may be considered that the region of low aftershock activity might be subjected to almost all the stress releases by a large dislocation.

As a coseismic dynamic effect in the source area, we will consider the percentage of collapsed houses. The results are shown in Fig.11-B(YAKUWA,et.al. 1928). These iso-collapse curves of houses indicate some degree of acceleration caused by the short-period waves. The contour lines indicate that the predominant short-period waves were not radiated uniformly nor

at random from the assumed fault with a length of 35km. It is most likely that the predominant short-period waves were mainly radiated from the relatively small region surrounded by the broken line.

This region also coincides with that characterized by a large dislocation and extremely low aftershock activity. As was mentioned in sections 2.3 and 2.6, if predominant short-period waves indicating high intensity are produced from the ruptures of many small elements, large amount of dislocation may be explained by the superposition of dislocations caused by many small faults.

3.3 The Northern Izu Earthquake of Nov.26, 1930(M=7.0)

The epicenters of aftershocks located by the Central Meteorological Observatory of Japan are shown in Fig.12-A. Although the epicenters determined are scant and some divergent because of the poor quality of the data from routine observations in the early 1930's, there was a low activity of aftershocks in the Tanna region surrounded by the broken line. On the basis of P-wave first motions and S minus P times recorded at the Mishima and Numazu stations, HAYATA(1931) suggested that a number of undetermined epicenters of aftershocks had occurred mainly in the region from Ukihashi to the Kano River.

KISHINOUE(1936) carried out the aftershock observations by using portable seismometers at Tanna, Ito and Mishima, and reported that the aftershock activity at Tanna was remarkably low. Based on these results, KISHINOUE(1936) interpreted that the region subjected to the greatest breakages was no longer affected by the tectonic stress, accordingly new fractures could

not take place in this region. His interpretation was quite similar to our comprehension that the aftershock activity is low in the region where many ruptures have already occurred.

Contours of equal maximum shear strains obtained by TSUBOI (1932b) and the surface dislocation compiled by MATSUDA(1972) are shown in Fig.12-C and 12-D, respectively. These static deformations indicate the maximum value around the Tanna region. The dynamic factores are shown in Fig.12-B in terms of the percentage of collapsed houses(KUNITOMI,1930). Although the distribution of collapsed houses shows a tendency to extend over a plane of thick alluvium, contour lines in Fig.12-B suggest that the region surrounded by a broken line has been subjected to a relatively large acceleration. From the results presented above, it may be concluded that the predominant short-period waves were radiated from the relatively small area around Tanna.

3.4 The Tottori Earthquake of Sep.10, 1943(M=7.4)

As was discussed in section 2, long-period and strong-motion seismograms of the main shock were obtained at a relatively short focal distance. In addition to these seismograms, detailed field data from triangulation surveys and aftershock activity are available for this study. Using the long-period seismograms and the geodetic data, KANAMORI(1972) has described the general features of the faulting process of this earthquake on the assumpion that the fault motion was a simple uniform dislocation.

Temporary mobile observation of the aftershocks began on Sep.14

by OMOTE(1955). The aftershock distribution shown in Fig.13-A indicates that the activity of aftershocks was extremely low in the central part of the main fault assumed by KANAMORI(1972). Before the begining of the temporaly observations, noticeable aftershocks including two prominent shocks with magnitudes of 6.1 occurred near Kurayoshi and the upper end of the Tenjin River(INOUE, 1943), which corresponds to the west end of the assumed fault. Aftershock epicenters in this early period were located by the Central Meteorological Observatory of Japan, but the accuracy was less than that from the temporary observations. Accordingly, the energies of the aftershocks immediately following the main shock are plotted with error bars of some degrees along the direction of the fault strike(the lower part in Fig.13-D). The energies released by aftershocks are calculated by use of the magnitudes and energies reletion(e.g. UTSU, 1977). The energy densities are low around Yoshioka and Shikano.

Coseismic static deformations are shown in Fig.13-C and the upper part of Fig.13-D. Triangulations data were compiled by SATO(1973) and the surface dislocations were surveyed by TSUYA(1944). From these figures the dislocation is confirmed to be maximum in the region of Yoshioka and Shikano. The isoseismals investigated by INOUE(1943) are shown in Fig.13-B. High seismic intensity extends over the Tottori plane and the coastal region because of a thick alluvium. It is, however, most likely that the highest intensity was not radiated all over the presumed fault but near the region indicated by a broken line in Fig.13-B. From the results presented above, the specific region radiating the predominan short-period waves is defined in a small area between Yoshioka and Shikano.

3.5 The Fukui Earthquake of June 28, 1948(M=7.3)

Since this earthquake occurred in the Fukui plane covered by a thick alluvium, static and dynamic field features were not as obvious as we had expected. Any clear fault offset was not found, but several ground fissures aligned en echelon indicated by hatched in Figs.14-A, 14-B and 14-C were found. Contours of maximum shear strains compiled by NASU(1950) suggest a considerable dislocation in bedrocks(Fig.14-C). Although the contour lines seem to define two regions, that is, the northern and southern parts of Maruoka, the amount of maximum shear strains is larger in the southern part. TAKAHASHI(1951) reported that a number of fissures with large dimensions were traced south and west of Maruoka.

Aftershock distribution was obtained from the data of temporary mobile observations(OMOTE,1950). Although the aftershock epicenters shown in Fig.14-A are rather scattered, it appears that the activity in the southern area(Fukui - Maruoka) along the assumed fault is a little less than that of the northern area. As collapsed houses(TAKAHASHI, 1951) were distributed over the Fukui plane as shown in Fig.14-B, it is difficult to define the region subjected to especially large accelerations. Although the surface features accompanying this earthquake are obscure, as mentioned above, the specific region for this earthquake may be defined in the small area between Fukui and Maruoka.

Another possible reason why coseismic and postseismic features are obscure may be confirmed by the fact that this was a typical multiple shock earthquake(KOSHIKAWA(1948), OGAWA(1949) and KOMUR (1958)). As shown in Fig.5, the first shock is followed by

the second shock after about 9sec. KANAMORI(1973) analyzed the long-period seismograms recorded at the Abuyama Seismological Observatory and concluded that the second shock was about four times larger than the first. However, short-period waves followed by the first shock are considerably larger than those of the second one as seen in Fig.5. Therefore, the region which radiated the predominant short-period waves, may coincide with that of the first shock. The starting points of the first and second ruptures were determined by KOSHIKAWA(1948), and they were located at about 4km north of Fukui and near Maruoka, respectively. As the relationship between the starting point and the ripple generating region will be discussed in Appendix A, it is most likely that this specific region concerned with the first shock was defined in the area between Fukui and Maruoka.

3.6 Other Earthquakes

The earthquakes occurring in oceanic areas, the lack of geological and geodetic data in the near fields prevents us to identify the ripple generating core. Quite recently, however, the precision of locating the aftershocks of large earthquakes occurring in oceanic areas(Fig.15) has increased, allowing us to define the low active aftershock regions.

The aftershock distribution of the Izu-Oki earthquake of May 8, 1974(M=6.9), which was obtained by the RESEARCH GROUP for AFTERSHOCKS(1975), showed a low activity zone in the central part of a belt-like zone of aftershock distribution with a length of about 30km. The low activity in the central part of the aftershock zone was also found by ISHIBASHI et.al.(1975) on the basis of the observation data obtained from a network of

ultra sensitive seismographs. They suggested that the stress in a low activity region of aftershock might have been almost completely released concurrently with the main shock.

The Izu-Oshima earthquake of Jan.14, 1978(M=7.0) occurred in an oceanic area between the Izu peninsula and the Izu Oshima island. The precise distribution of aftershocks was obtained by TSUMURA et.al.(1978). The belt-like distribution of aftershocks extended to about 40km across the Izu peninsula, but the aftershock activity was extremely low around the starting point of the main shock i.e. the sea bottom. From data of isoseismals and distribution of disasters on the Izu peninsula, UMEDA and MURAKAMI(1978) suggested that the strongest acceleration was radiated from a low activity zone of aftershocks between the Izu peninsula and the Izu Oshima island.

The earthquakes discussed in this section are all intra-plate earthquakes with nearly strike-slip motions. For several major inter-plate earthquakes with low-angled reverse-slip motion, KATSUMATA and YOSHIDA(1980) reported that there were seismic gaps in the aftershock regions. It is suspected that these seismic gaps correspond to the ripple generating cores as discussed in this paper.

4. The Source Model with a Ripple Generating Core

4.1 Multiple Rupture

We will discuss the rupture process in the ripple generating core and propose a source model to explain the observed seismic waves. As already mentioned, it is basically considered that the short-period and the long-period waves are radiated from small rupture elements within the ripple generating core and from a smoothing rupture process over the main fault,respectively. In order to simplify the model, we assume that each rupture element within a ripple generating core has the same fault geometry and the same fault motion as the main fault, and that these rupture planes are arranged in parallel each other in the vicinity of the main fault. For the first step, we have to estimate the order of length(ℓ), width(w) and dislocation (d) of small faults, and for a second step, we have to determine the number of small ruptures and the time processes of rupture so as to explain the observed seismic waves.

As an example, we will discuss the Tottori earthquake of 1943, for which broad-band seismograms and spectrum deduced from the seismograms at the Abuyama Seismological Observatory (Δ=140km) are shown in Figs.3 and 4. The predominant periods of short- and long-period waves are t=0.3$\sim$0.5sec and T=15sec, respectively. We adopt the period ratio p=T/t=30$\sim$50 as a scaling factor. If dynamic rupture parameters in terms of the rise time and rupture velocity on the small faults satisfy the conditions discussed in section 5.1, the dimensions of a small faults and the dislocation may be scaled as ℓ=L/p, w=W/p and d=D/p on the basis of the scaling law(AKI, 1967),

where L,W and D are the length, width of the main fault and its dislocation, respectively. With reference to the above relations, the dimensions of small faults and the dislocation on it are taken as shown in the table inserted in Fig.16. A wavelet radiated from a small faulting has been computed by the use of HASKELL's method(1969), which gives the displacements in an infinite homogeneous medium. The expected wavelet at the Abuyama Seismological Observatory is shown in Fig.16-A. The very small amplitude of this wavelet is of course as expected from the scaling law, which implies that the amplitude of the wavelet with a period of T/p is reduced to A/p^3, where T and A are the period and amplitude of long-period waves, respectively. Accordingly, to obtain a large amplitude of short-period waves, we assume that some of many small elements rupture almost simultaneously in a ripple generating core and that the seismic waves radiated from each faulting are superposed in the propagating medium. In the case of the Tottori earthquake, the number for these simultaneous ruptures is given as shown in Fig.16-A.

4.2 Time Process of Faulting

In order to simplify the treatments, instead of taking the phase delay time of each faulting, we assume that simultaneous rupture groups slip successively with a certain interval. This interval time is taken to be longer than the process time of small rupture, but not to be so long as to disrupt the short-period duration of wavelets. In the case of the Tottori earthquake, this interval time is taken as shown in Fig.16-B. The rupture groups having these intervals break out in succession within the duration(τ_s) of short-period waves(Fig.16-B)

Actually, the rupture processes in the ripple generating core may be more complex. But the two most essential assumptions are only taken into account in this paper for simplicity of the model. The simultaneous rupture is necessary to explain the large amplitudes of observed short-period waves, and the successive ruptures produce the duration of short-period waves or the spectral peak in the frequency domain.

The ground displacements at an observation point are the sum of displacements due to short-period waves and long-period waves radiated from the ripple generating core and from the main fault, respectively. For the Tottori earthquake, the N-S component of ground displacement at the Abuyama Seismological Observatory is shown in Fig.16-C. The source parameters of the main fault are the same as those obtained by KANAMORI(1972). The calculated spectrum of ground displacement is shown in Fig.17. The spectral peak around 2.5Hz is similar to the one shown in Fig.4. The synthetic seismograms are computed by convolving the ground displacements with the impulse response of low magnification long-period and strong-motion seismographs, respectively. These result are shown in Fig.18. The crustal amplification as described in section 2.4 was not taken into account for computing the above seismograms, ground displacement and spectra. If this revision is taken into account, the results shown in Fig.18 will explain the observed results(Fig.3) for long-period and predominant short-period seismic waves. But the observed coda waves following the parts of τ_S cannot be explained by the present calculations.

5. Discussions

5.1 Some Conditions on the Rupture of Small Faults

In the preceding two sections, in order to explain the recorded short-period waves, only static fault parameters such as the fault dimensions and dislocation were varied according to the scaling law. Now, we will estimate conditions of dynamic parameters such as the rise time(τ) and rupture velocity(v). The rupture with short rise time and large rupture velocity would concentrate the seismic energy radiation in a short time, and hence, produce a relatively large amplitude and short-period wavelet.

In this case, however, the dynamic fault parameters should be limited to within some reasonable ranges. OTSUKA(1976) indicated that the maximum particle velocity deduced from the upper limit of crustal strain $\sim 10^{-4}$ was 40$\sim$50cm/sec. This maximum value of particle velocity was also shown by various observations at the source region(MURAMATSU, 1976). These results may express particle velocities of seismic waves propagating in a medium, but they also imply that there exists the upper limits of dynamic rupture parameters in the earth's crust. Therefore, we will accept the conditions that $v \lesssim \beta$ and $d/2\tau$ (particle velocity) $\lesssim$ 50cm/sec, where β is the shear wave velocity and d is the amount of dislocation. In the preceding two sections, the above limits of dynamic fault parameters have been taken into account. Since these upper limits of dynamic parameters restrict energy concentration in a short time, it is difficult to obtain high efficency of short-period waves

We attempt to examine the wave forms for other case of static fault parameters. In the same way as in the previous section,

the wave forms at Abuyama are calculated for the ruptures at Tottori. The rupture over one fault with a large dislocation and small dimensions of d=2.5m, ℓ=1km and w=1km radiates a wavelet having the process time of about 3.5sec. When this wavelet is superposed with certain interval times, long-period seismic waves are generated. But the amplitude of the short-period waves is negligible.

5.2 Stress Release and Total Deformation in and around the Ripple Generating Core

It is not necessary for our model to assume that the effective stress or the stress drop on a single rupture element in the ripple generating core is especially high. The effective stress(σ) is expressed by KANAMORI(1972), as

$$\sigma = \mu d\sqrt{1-(v/\beta)^2}/(\pi v\tau)$$

, where μ;rigidity, d;dislocation of small fault and β;shear wave velocity. In our model, the rupture velocity(v) and particle velocity($d/2\tau$) are restricted by the upper values as described in the previous section. Thus, the effective stress driving each small rupture element is of the same order as that of the main fault.

The stress drop $\Delta\sigma$ for each rupture is expressed by using the average dislocation(d) and fault width(w) as follows,

$$\Delta\sigma = c\mu d/w$$

, where c is a constant. In our model, the stress drop for each rupture is not especially high nor low, because both of the fault dimensions and fault dislocation are in accordance with those expected from the scaling law of earthquakes. It should

be understood that a large number of rupture elements with normal stress drop are distributed in the ripple generating core. The extremely low activity of aftershocks in this region may be possibly explained by the arguments given in this section.

As was expected in section 3.1, the observed deformations around the ripple generating core are fairly large in comparison with those of all other portions of the main fault. This result implies that a number of small faults must be rather close to each other and do cause an accumulative dislocation. Because, if these small faults are at distances from each other, for example ten times the lengths of their faults, the dislocations on each small fault would not be accumulated.

6. Conclusion

The rupture processes of large shallow earthquakes have been investigated on the basis of broad-band seismograms recorded at relatively short focal distances as well as of coseismic and postseismic spatial features which have been surveyed near the source regions.

It is generally accepted that long-period and short-period seismic waves represent a uniform faulting process and a finer rupture process, respectively In order to obtain the detailed source mechanism, predominant short-period waves have been mainly investigated by comparison with long-period waves. The characteristic features of these short-period waves on seismograms are summarized as follows.

1. The periods of the predominant short-period waves are completely separated from those of long-period waves. In the frequency domain, these waves have a peak at high frequencies.
2. The amplitudes of short-period waves are extremely large in comparison with those expected from the smoothing dislocation of a single main fault.
3. The durations of these short-period waves are concentrated in the initial parts of P- and S-waves.

From the above facts, a possible rupture process radiating the predominant short-period waves may be considered as follows. A large number of small ruptures occur at an early stage of the smoothing dislocation on a main fault and terminate in a relatively short time. It is, further, speculated that these ruptures are concentrated within a relatively small region.

In order to confirm this speculation, coseismic and postseismic

spatial phenomena at near focal regions have been investigated for some of large shallow earthquakes that have occurred in Japan. The obtained results show that there exists a specific region characterized by the following field features.

1. Aftershock activity immediately after the main shock occurrence is extremely low within the specific region.
2. Static dislocations observed geodetically and geologically are especially large in and around the specific region.
3. Dynamic factors such as isoseismals or the distribution of collapsed houses are centered in the specific region.
4. The dimension of this specific region may be considerably small in comparison with that of the main fault, although its boundaries are not clear.

This specific region has been named " a ripple generating core " in an earthquake source area.

On the basis of the observational results mentioned above, an earthquake source model with a ripple generating core has been proposed. The dislocation theory and earthquake scaling law have been applied to each faulting, and the static fault parameters of small faults in the concerned regions have been estimated from the period ratio(p) of long- to short-period waves. The dynamic fault parameters in terms of the rise time(τ) and the rupture velocity(v) have been restricted by $d/2\tau \lesssim 50$cm/sec and $v \lesssim \beta$. So long as our model is based on the above conditions, the stress drop($\Delta\sigma$) and effective stress(σ) concerned with each small fault have nearly the same order as those of the main fault.

The time processes of rupture within the ripple generating core are supposed that some of the many small elements rupture simultaneously and this situation proceeds for a certain interval

of time. The observed seismic waves are the sum of short- and long-period waves radiated from the ruptures within the ripple generating core and from the dislocation of the main fault. The synthetic seismograms calculated under these conditions well explain the periods and amplitudes of the observed seismograms.

Some intra-plate earthquakes have been mainly discussed in this paper. The ripple generating core expressed in terms of predominant short-period waves and an extremely low activity of aftershocks will be revealed in some of the inter-plate earthquakes in Appendix A. Existance of the ripple generating core in transform fault earthquakes remain verified. For future studies, we have to investigate the preseismic and coseismic roles in this specific regions. For an understanding of the physical processes of earthquakes, it is important to know how the ripple generating core develops in an earthquake source area.

Acknowledgments

The author wishes to thank Professor H.MIKI and Dr. H.WATANABE for their helpful advice and critical readings of the manuscript throughout this study. He also wishes to thank Mr. I.HIRANO and Mr. K.ITO for their useful comments for the computation of wave forms.

Appendix A. Starting Point of the Rupture and Ripple generating Core

Predominant short-period waves are observed at a short time(t_d) after the onset of P- and S-waves, as is shown in Figs.3,5 and 6. It will be shown, in this section, that this fact can be widely detected in some of the recent earthquakes(Fig.15). The initial parts of seismograms recorded by electromagnetic seismograms with a flat responses from 0.1 to 5sec and V=100, from the Japan Meteorological Agency, are shown in Fig.19.

It is noticed that the predominant short-period waves discussed now suddenly increase after a duration of waves of a rather long-period and relatively low amplitudes. The time intervals between the onset of the P-wave and the predominant short-period waves are plotted against distances in Fig.20. The time lag(td) inherent to each earthquake is clearly found regardless of epicentral distances. This fact strongly suggests that the formation of ripple generating core begins a little later than the start of the smoothing dislocation which radiates the long-period waves.

Another possibility is that the ripple generating core may be located at some distance from the starting point of the rupture which radiates the initial P-wave. From the Izu-Oshima earthquake of Jan.14,1978(M=7.0), SHIMAZAKI and SOMERVILLE(1979) concluded that the main shock occurred approximately 6sec after a precursory event, and also that the starting point of the precursory event was about 4km east of the main shock. As already described in section 3.6, UMEDA and MURAKAMI(1978) suggest that large accelerations were radiated from a relatively small region including the main shock, which corresponded to an extremely low activity region of aftershocks. Accordingly, it is very likely that

the ripple generating core of this earthquake was located at some distance from the starting point of the main rupture.

From the Tokachi-Oki earthquake of May 16,1968(M=7.9) and the Etorofu earthquake of Oct.13,1963(M=8.1), NAGAMUNE(1971) suggested that strongest waves were radiated from the secondary rupture points which were located 107km west and 130km north-east from the starting points, respectively. KATSUMATA and YOSHIDA(1980) named the regions including the above secondary rupture points " the core of the focal region " because of low seismic activity before and after the main shocks. Thus, it is quite possible that this region was also at some distance from the starting point of the main faulting.

Appendix B Spectra of Earthquakes with Various Magnitudes

The ripple generating core associated with large shallow earthquakes have so far been discussed, because field features of the specific regions were conspicuously revealed only by the large earthquakes. For earthquakes of various sizes, we investigate spectral peaks at high frequencies which are one of the characteristic features of the ripple generating system. The spectra of seismic P-waves obtained by analogue band-pass filters are shown in Fig.21. Seismograms of small and micro-earthquakes($M < 5$) were recorded at short focal distances within about 35km by a portable broad-band seismograph system(UMEDA,1973 and UMEDA,1975). Large and moderate earthquakes ($M \geq 5$) were recorded at the Abuyama Seismological Observatory by the system described in section 2.1.

Since these earthquakes($M \geq 5$) have different focal distances from 40km to 170km, the spectra plotted in Fig 21 are corrected

for attenuation and geometrical spreading of waves at a referance distance of 35km using the following equation.

$$A = A_o r^{-1} \exp(-2\pi fr/Q\alpha)$$

,where r;focal distance(km), f;frequency(Hz) and α;P-wave velocity. Q-value and P-wave velocity are given as Q=500 and α=6.0km/sec, respectively.

As has been already explained for the case of large earthquakes, the seismic spectrum has two peaks at low and high frequencies. The two spectral peaks, as seen in Fig.21, vary with earthquake magnitude indicating two trends. One of the trends at low frequencies appears proportional to f^{-3}, corresponding to that expecte theoretically from the scaling law for a smoothing dislocation model (e.g. AKI,1967). The other trend seems to be almost invariable with the earthquake's magnitude. The latter trend can be found only in the case of larger earthquakes with magnitudes of 3 or more. This trend at high frequencies implies that the representative rupture dimension radiating the predominant short-period waves might correspond to that of earthquakes with a magnitudes of about 3.

The spectral amplitudes for both low and high frequencies increase with the earthquake's magnitude. The low frequency amplitude can be explained by the increase of fault dimensions and fault dislocation, while the latter may be explained by the increased number of ruptures having representative dimensions.

For earthquakes with magnitude smaller than 3, the seismic waves radiated from one fault plane would produce most effectively to the high frequency spectral amplitudes. It may be considered that the ripple generating core does not develop in these small or micro-earthquakes.

As seen for earthquakes with M$\sim$5 in Fig.21, the spectral peak at high frequencies is not always prominent. These examples indicate that a distinctive ripple generating core is not always formed for all earthquakes. The scaling of earthquake spectra obtained by the present observation data is still incomplete. Broad-band spectra for large earthquakes and high frequency spectra for urtra-microearthquakes must be investigate in more detail.

References

ABE,K., Dislocations,source dimensions and stresses associated with earthquakes in the Izu peninsula, Japan, J.Phys.Earth., 26, 253-274, 1978.

AKI,K., Scaling law of seismic spectrum, J.Geophys.Res.,72,1217-1231, 1967.

DAS,S. and K.AKI, Fault plane with barriers; a versatile earthquake model,J.Geophys.Res.,82,5658-5670, 1977.

HASKELL,N.A., Elastic displacements in the near-field of a propagating fault,Bull.Seismol.Soc.Am.,59,865-908,1969.

HARTZELL,S. and J.N.BRUNE, The Horse canyon earthquake of August 2, 1975—two-stage stress-release process in a strike-slip earthquake,Bull.Seismol.Soc.Am.,69,1161-1173,1979.

HAYATA,K., The epicenters of fore- and aftershocks of the large Northern Izu earthquake, Kenshinjiho(Quart.J.Seismol.),5, 123-130, 1931(in Japanese)

INOUE,W., The general features of the Tottori earthquake of Sep.10, 1943, Kenshinjiho(Quart.J.Seismol.), 15-27, 1943(in Japanese).

ISHIBASHI,K., K.SUYEHIRO, H.INATANI, T.MATSUZAKI and T.ASADA, Ultra sensitive observation of aftershocks of the earthquake off Izu peninsula,May 9,1974, ed. R.TSUCHI,21-26, Rep.Earthq. off the Izu Peninsula,1974 and the Disaster,1975(in Japanese).

ITO,K. and H.MURAKAMI, The crustal structure in northern Kinki district,The Studying Results of Natural Disaster Science No.A-53-5, ed.H.MIKI, 1978(in Japanese)

KANAI,K., Earthquake Engineering,p72, Kyoritsu-Shyuppan,Tokyo, 1975(in Japanese)

KANAMORI,H., Determination of effective tectonic stress associated with earthquake faulting, the Tottori earthquake of 1943, Phys.Earth Planet.Interiors,5,426-434, 1972.

KANAMORI,H., Mode of strain release associated with major earthquakes in Japan, Ann.Rev.Earth Planet Sci., 1,213-239, 1973.

KATSUMATA,M. and A.YOSHIDA, Change in seismicity and development of the focal region, Pap.Meteorol.Geophs.,31,15-32,1980.

KISHINOUE,F., On the fore- and aftershock distribution of the Izu earthquake of 1930, Zisin(J.Seismol.Soc.Japan),i,8,12, 1-7,1936(in Japanese).

KOMURA,S., A consideration about the mechanism of occurrence of large-scale earthquakes,1, Mem.Coll.Sci.Univ.Kyoto, Ser.A,28,363-378,1958.

KOSHIKAWA,Y. Seismometrical study of the Fukui earthquake. The Fukui Earthquake of June 28,1948, ed.H.TSUYA, 30-36, Committee for the Study of the Fukui Earthquake, 1948.

KUNITOMI,S., The general report of northern Izu earthquake, Kenshinjiho(Quart.J.Seismol.),4,257-260, 1930.

MATSUDA,T., Active faults and earthquakes—the geological aspect, The Memoirs of the Geological Society of Japan—fault and earthquake—,chief editor;K.HUZITA, 12,15-32, 1976(in Japanese)

MATSUDA,T., Surface faults associated with Kita-Izu earthquake of 1930 in Izu peninsula, Japan, in Izu Peninsula, eds.M.HOSHINO and H.AOKI, 73-93, Tokai Univ.Press, 1972(in Japanese)

McGARR,A., S.M.SPOTTISWOODE and N.C.GAY, Observations relevant to seismic driving stress, stress drop and efficiency, J.Geophys. Res.,84,2251-2261,1979.

MIKUMO,T. and T.MIYATAKE, Dynamical rupture process on a three-dimensional fault with non-uniform frictions and near-field seismic waves, Geophys.J.R.astr.Soc.,54,417-438, 1978.

MIZUTANI,S. and Y.KANAORI, Faulting process, Kagaku,46,536-544, Iwanami Tokyo,1976(in Japanese).

MURAMATSU,I., The maximum value and the duration of the strong earthquake motion, Zisin(J.Seismol.Soc.Japan),ii,29,223-232, 1976(in Japanese).

NAGAMUNE,T., Source regions of great earthquakes, Geophys.Mag., 35,333-399, 1971.

NAKAMURA,S., The report of the Oku-Tango earthquake, Saito-hoonkai, Science report,5, Sendai,1928(in Japanese).

NASU,N., On the aftershocks of the Tango earthquake, Bull.Earthq. Res.Inst.,6,245-332, 1929-a(in Japanese).

NASU,N., Further study of the aftershocks of the Tango earthquake, Bull.Earthq.Res.Inst.,7,133-152, 1929-b(in Japanese).

NASU,N., Supplementary study on the stereometrical distribution of the aftershocks of the great Tango earthquake of 1927, Bull.Earthq.Res.Inst.,13,335-399, 1935.

NASU,N., Crustal deformation, The Fukui Earthquake of June 28, 1948, ed.H.TSUYA,93-123, Committee for the study of Fukui Earthquake, 1950.

OGAWA,M., Seismic vibration of the Fukui earthquake observed at the Abuyama Seismological Observatory, Bull.Disaster Prev.Inst.Kyoto Univ.,2,122-123, 1949.

OKANO,K. and Y.UMEDA, Continuous observation of crustal deformation at Abuyama Seismological Observatory, Zisin(J.Seismol.Soc. Japan),ii,27,262-269,1974(in Japanese).

OMOTE,S., Aftershocks, The Fukui Earthquake of June 28,1948, ed.H.TSUYA,37-78, Comittee for the Study of Fukui Earthquake, 1950.

OMOTE,S., Aftershocks that accompanied the Tottori earthquake of Sep.10,1943(the 2nd paper), Bull.Earthq.Res.Inst., 33,641-661, 1955.

OTSUKA,M., A simulation of earthquake occurrence part 5 an interpretation of aftershock phenomena, Zisin(J.Seismol. Soc.Japan),ii,29,137-145, 1976(in Japanese).

RESEARCH GROUP FOR AFTERSHOCKS, Observation of the main and aftershocks of the earthquake off the Izu peninsula,1974, ed.R.TSUCHI,11-19,Rep.Earthq.off the Izu Peninsula,1974 and the Disaster, 1975(in Japanese).

SASSA,K., The preliminary report of the Abuyama Seismological Observatory, Chikyu-Butsuri(Geophysics), Geophys.Inst. Kyoto Univ.,5,No1,1-3, 1941(in Japanese)

SATO,H., A study of horizontal movement of the earth crust associated with destructive earthquakes in Japan, Bull. Geograph.Surv.Inst.,Tokyo,19,89-130, 1973.

SHIMAZAKI,K. and P.SOMERVILLE, Static and dynamic parameters of the Izu-Oshima, Japan earthquake of January 14,1978, Bull.Earthq.Res.Inst.,69,1343-1378, 1979.

TAKAHASHI,R., Brief reports of the Fukui earthquake, Reports of Disasters from the Fukui Earthquake, part II., concerning architecture, The Special Committee for the Study of Disasters from the Hokuriku Earthquake, 1-22, 1951(in Japanese).

TSUBOI,C., Investigation on the deformation of the earth's crust in the Tango district connected with the Tango earthquake of 1927.(part 4), Bull.Earthq.Res.Inst.,10, 411-434, 1932-a.

TSUBOI,C., Investigation on the deformation of the earth's crust in Izu peninsula connected with the Izu earthquake of Nov.26,1930, Bull.Earthq.Res.Inst.,10,436-448, 1932-b.

TUMURA,K., I.KARAKAMA, I.OGINO and M.TAKAHASHI, Seismic activities before and after the Izu-Oshima-kinkai earthquake of 1978, Bull.Earthq.Res.Inst.,53,675-706, 1978(in Japanese).

TSUYA,H., The Shikano and Yoshioka faults and geology of the region affected by the Tottori earthquake of 1943, Bull.Earth. Res.Inst.Tokyo Univ.,22,1944(in Japanese).

UMEDA,Y., Observation of long-period seismic waves at a short distance from the focal area, Zisin(J.Seismol.Soc.Japan), ii,26,336-347, 1973(in Japanese).

UMEDA,Y., Observation of long-period seismic waves at a short distance from the focal area(part 2), Zisin(J.Seismol. Soc.Japan),ii,28,313-320, 1975(in Japanese)

UMEDA,Y. and H.MURAKAMI, A cataclysmal line accompanying the 1978 near Izu-Oshima earthquake and disastrous features by the largest aftershock in Izu peninsula, Zisin(J.Seismol. Soc.Japan),ii,31,275-286, 1978(in Japanese).

UTSU,T., Seismology,Kyoritsu-Zensho p.128, Kyoritsu-Shyuppan, Tokyo,1977(in Japanese).

WATANABE,H. and H.SATO, Geological survey of the Tango earthquake, Geological Survey of Japan,100,1-102, 1928(in Japanese).

YAKUWA,R., S.TAKATANI, S.ICHIKI and K.TANAHASHI, The field survey of the northern Tango-earthquake(1st report), Kenshinjiho(Quart.J.Seismol.),3,143-168, 1928(in Japanese).

YAMASAKI,N. and F.TADA, The Oku-Tango earthquake of 1927, Bull. Earthq.Res.Inst.,4,159-177, 1928.

YOSHII,T., T.SASAKI, T.TADA, H.OKADA, S.ASANO, I.MURAMATSU, M.HASHIZUME and T.MORIYA, The third Kurayoshi explosion and the crustal structure in the western part of Japan, J.Phys.Earth,22,109-121, 1974.

Figure Captions

Fig.1 The response curves of long-period low-magnification (thick curves) and strong-motion(thin curves) seismograms. The numerals indicate the age when the response was adopted.

Fig.2 Location of earthquakes($M>5$) which occurred during the period from 1938 to 1975 at relatively short distances ($\Delta<200$km) and recorded by the broad-band seismograph at the Abuyama Seismological Observatory. The seismograms of named earthquakes are shown in Figs.3,5 and 6.

Fig.3 An example of broad-band seismograms for a large earthquake recorded at the Abuyama Seismological Observatory. T_o; the free period, ε; the damping ratio, V; the magnification of seismograph. τ_S and τ_L are the duration times of predominant short- and long-period seismic waves. t_d is the time lag (see Appendix A).

Fig.4 An example of the spectrum of observed ground displacements. A broken line indicates a slope of f^{-2}. (P-wave, N-S component of the Tottori earthquake).

Fig.5 An example of broad-band seismograms. For seismograph constants and other parameters, see caption in Fig.3. This earthquake represents a multiple shock.

Fig.6 Example seismograms and broad-band spectra. For the parameters in these figures, see caption in Figs.3 and 4. The spectrum of P-wave(lower left side) was obtained by using only a strong-motion seismogram.

Fig.7 Crustal response for the plane P-waves with incident angle of 90°. In the inserted table, ρ;density, α;P-wave velocity, H;thickness of layer

Fig.8a Some examples of strong-motion seismograms at relatively short focal distances. τ_S and τ_L are the duration times of predominant short-period and relatively long-period waves, respectively.

Fig.8b

Fig.9 The comparison of τ_S and τ_L, and the relation of these duration times and various earthquake magnitudes.

Fig.10 Schematic representation of " a ripple generating core " (surface projection).

Fig.11 Some surface phenomena suggesting the ripple generating core of the Tango earthquake of 1927, A) aftershock distribution (Mar.12-17,1927), after NASU(1935), B) percentage of collapsed houses(YAKUWA et.al.,1928), C) lines of equal maximum shear strain(TSUBOI,1932a) and D) surface dislocation along the fault(MATSUDA,1976). An elliptical area bounded by a broken line shows the ripple generating core of this earthquake. A solid thin line is an assumed fault(KANAMORI, 1973). ⊔⊔⊔ indicates the surface faults projected by this earthquake. The area indicated by shading in figure(B) is alluvium or alluvium-like.

Fig.12 Some surface phenomena suggesting the ripple generating core of the Northern Izu earthquake of 1930, A) aftershock distribution(Nov.26-Dec.31), after HAYATA(1931), B) percentage of collapsed houses(KUNITOMI,1930), C) lines of equal maximum shear strain(TSUBOI, 1932b) and D) fault displacements(MATSUDA,1972),

An elliptical area bounded by a broken line shows the ripple generating core of this earthquake. The thick lines and straight thin lines show the observed surface breakages

(MATSUDA, 1972) and assumed seismic fault(ABE,1978), respectively. The area indicated by shading in figure(B) is alluvium or alluvium-like.

Fig.13 Some surface phenomena suggesting the ripple generating core of the Tottori earthquake of 1943, A) aftershock distribution(Sep.14-28,1943), after OMOTE(1955), B) isoseismals(INOUE,1943), C) triangulation(SATO,1973) and D) upper;surface displacements(TSUYA,1944), lower; aftershock energy. An elliptical area bounded by a broken line shows the ripple generating core of this earthquake. The solid straight line and some thick broken curves show an assumed fault(KANAMORI,1972) and observed surface faults (TSUYA,1944), respectively. In figure(B), numerals attached to the isoseismals indicate intensities in J.M.A scale and the shading shows the alluvium or alluvium-like area.

Fig.14 Some surface phenomena suggesting the ripple generating core of the Fukui earthquake of 1948, A) aftershock distribution (July5-31,1948), after OMOTE(1950), B) percentage of collapsed houses(TAKAHASHI,1951) and C) lines of equal maximum shear strain(NASU,1950) An elliptical area bounded by a broken line shows the ripple generating core of this earthquake. The solid straight line and hatching show an assumed fault(KANAMORI,1973) and fissures on the surface (NASU,1950), respectively. The area indicated by shading in figure(B) is alluvium or alluvium-like area.

Fig.15 Location of earthquakes. Named squares correspond to Figs.11-14.

Fig.16 Inserted table; assumed fault parameters of main and

small faults. The expected wave form of the initial part of N-S component at the Abuyama Seismological Observatory for the Tottori earthquake. (A); a wavelet radiated from one small fault. (B); time series of successive faulting. (C); summation of the waves radiated from multiple ruptures and main faulting.

Fig.17 The spectrum of Fig.16-(C).

Fig.18 Synthetic long-period and strong-motion seismograms at the Abuyama Seismological Observatory for the Tottori earthquake of 1943.

Fig.19 Some seismograms observed at J.M.A stations for two recent earthquakes. First and second arrows in each seismogram indicate the initiation of smoothing rupture and of multiple rupture, respectively.

Fig.20 Time lag(t_d) versus distances. Circles and triangles indicate that the time lag is clearly defined or not clearly define because of long distances, respectively.

Fig.21 Broad-band seismic spectra observed at relatively short focal distances. The straight line indicates a slope of f^{-3} and each spectral peak at high frequencies is indicated by the broken line.

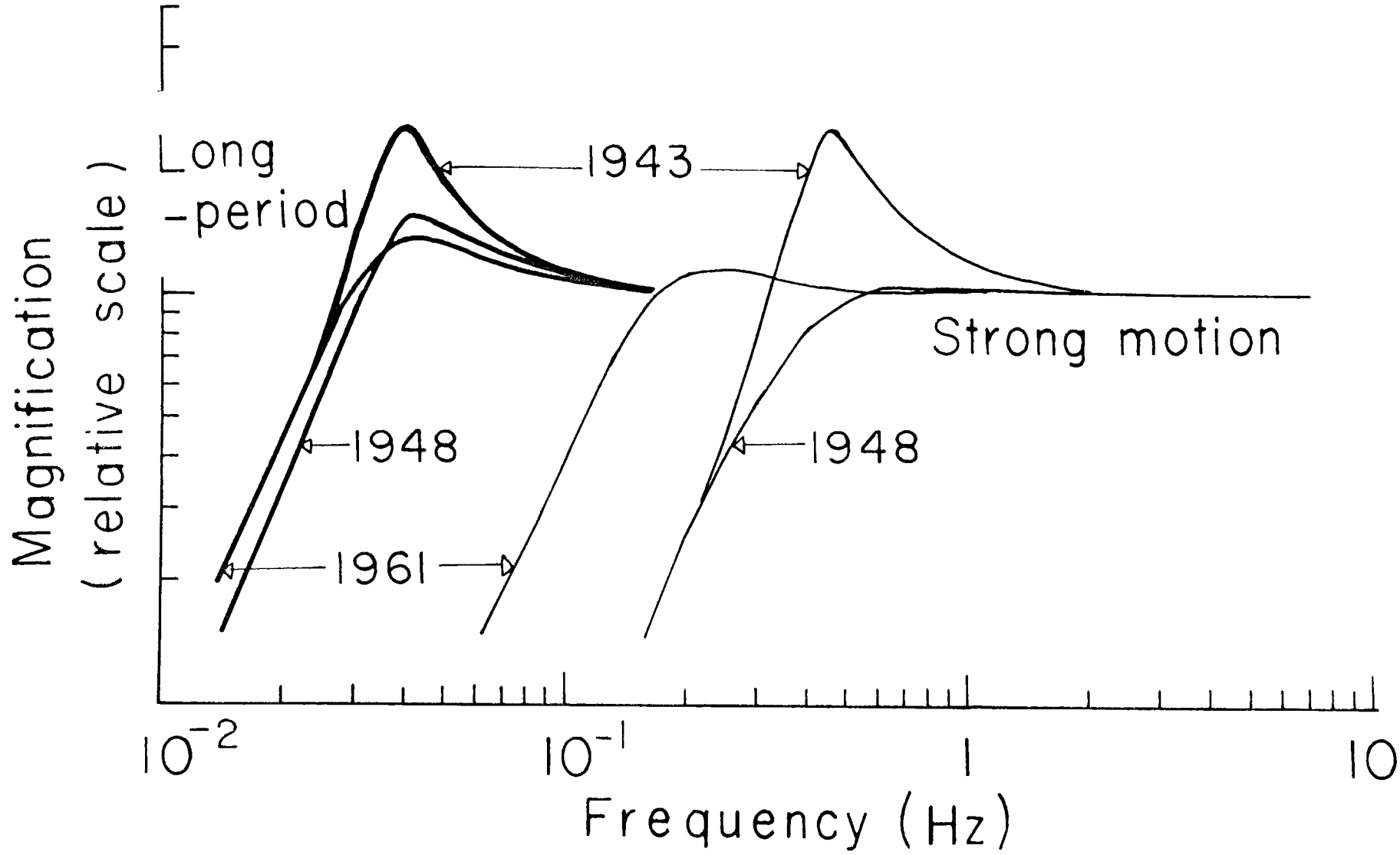
Long
-period
1943
Strong motion
1948
1948
1961
Magnification
(relative scale)
10^{-2}
10^{-1}
1
10
Frequency (Hz)

Fig.1

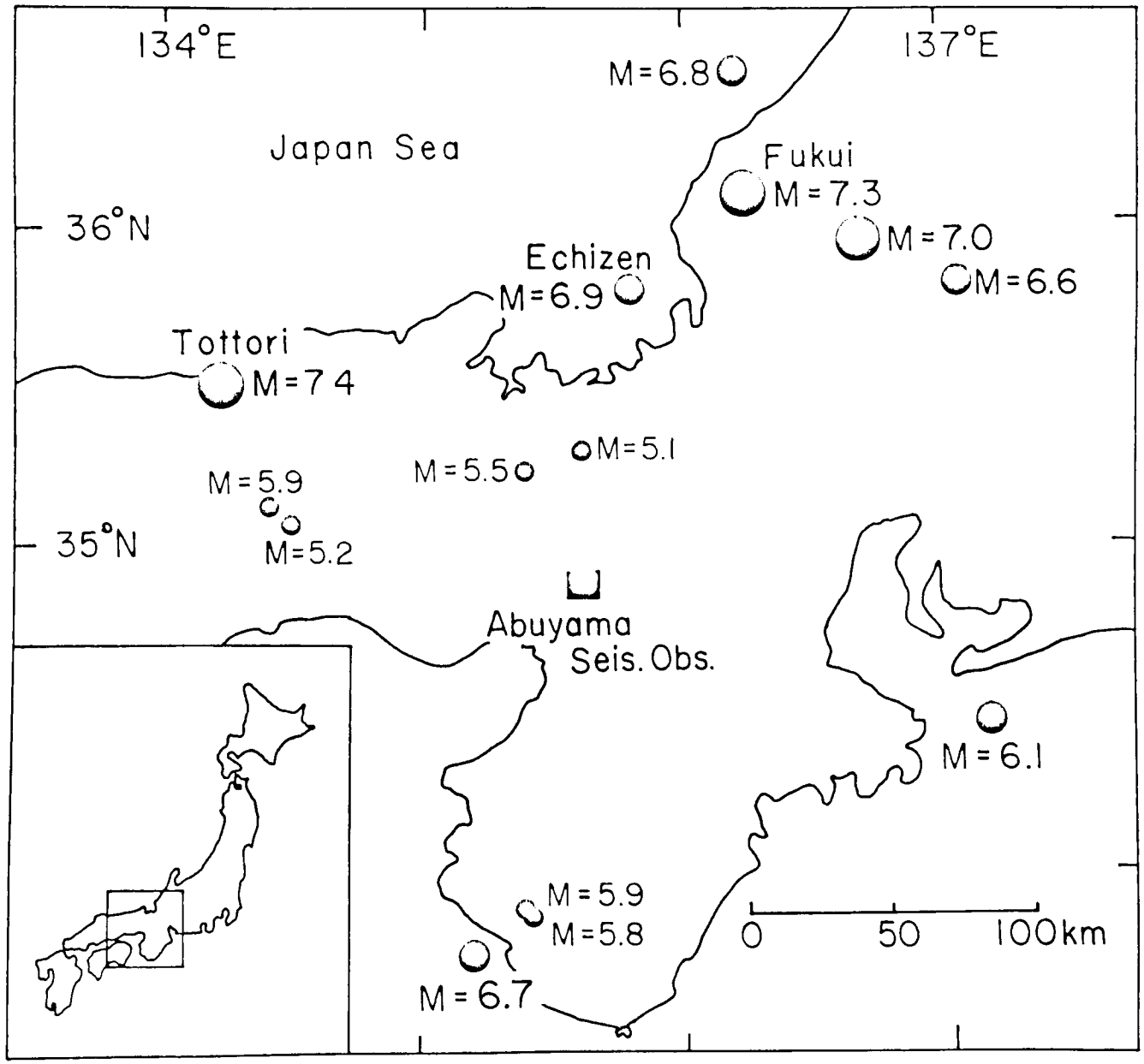
134°E
137°E
M=6.8
Japan Sea
Fukui
M=7.3
36°N
M=7.0
M=6.6
Echizen
M=6.9
Tottori
M=7.4
M=5.1
M=5.5
M=5.9
35°N
M=5.2
Abuyama
Seis. Obs.
M=6.1
M=5.9
M=5.8
M=6.7
0
50
100km

Fig.2

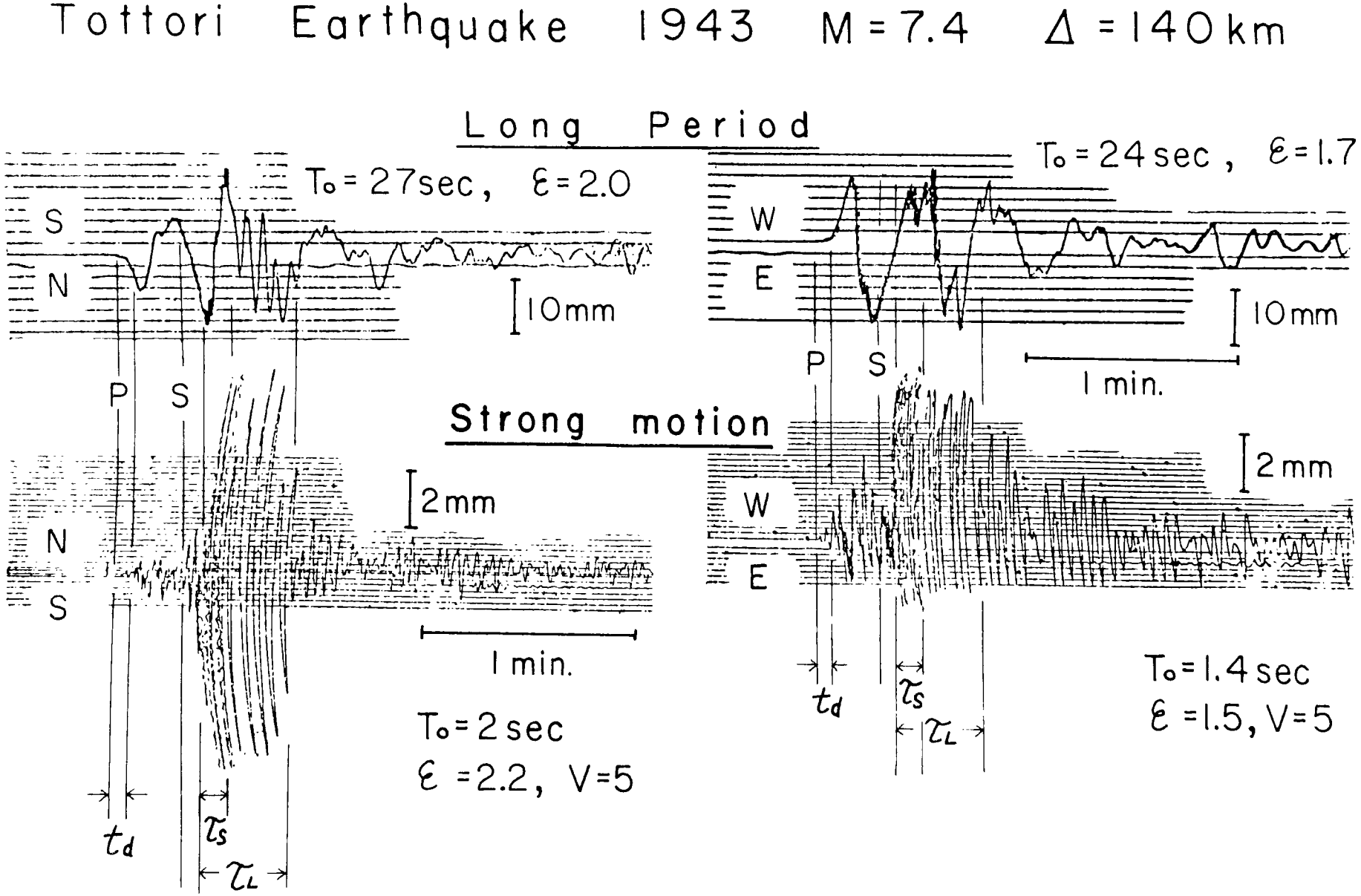
Tottori Earthquake 1943 M = 7.4 Δ = 140 km
Long Period
T₀ = 27 sec, ε = 2.0
S
N
10 mm
P
S
T₀ = 24 sec, ε = 1.7
W
E
10 mm
1 min.
Strong motion
2 mm
N
S
1 min.
T₀ = 2 sec
ε = 2.2, V = 5
W
E
2 mm
T₀ = 1.4 sec
ε = 1.5, V = 5
t_d
τ_s
τ_L

Fig.3

Fig.4

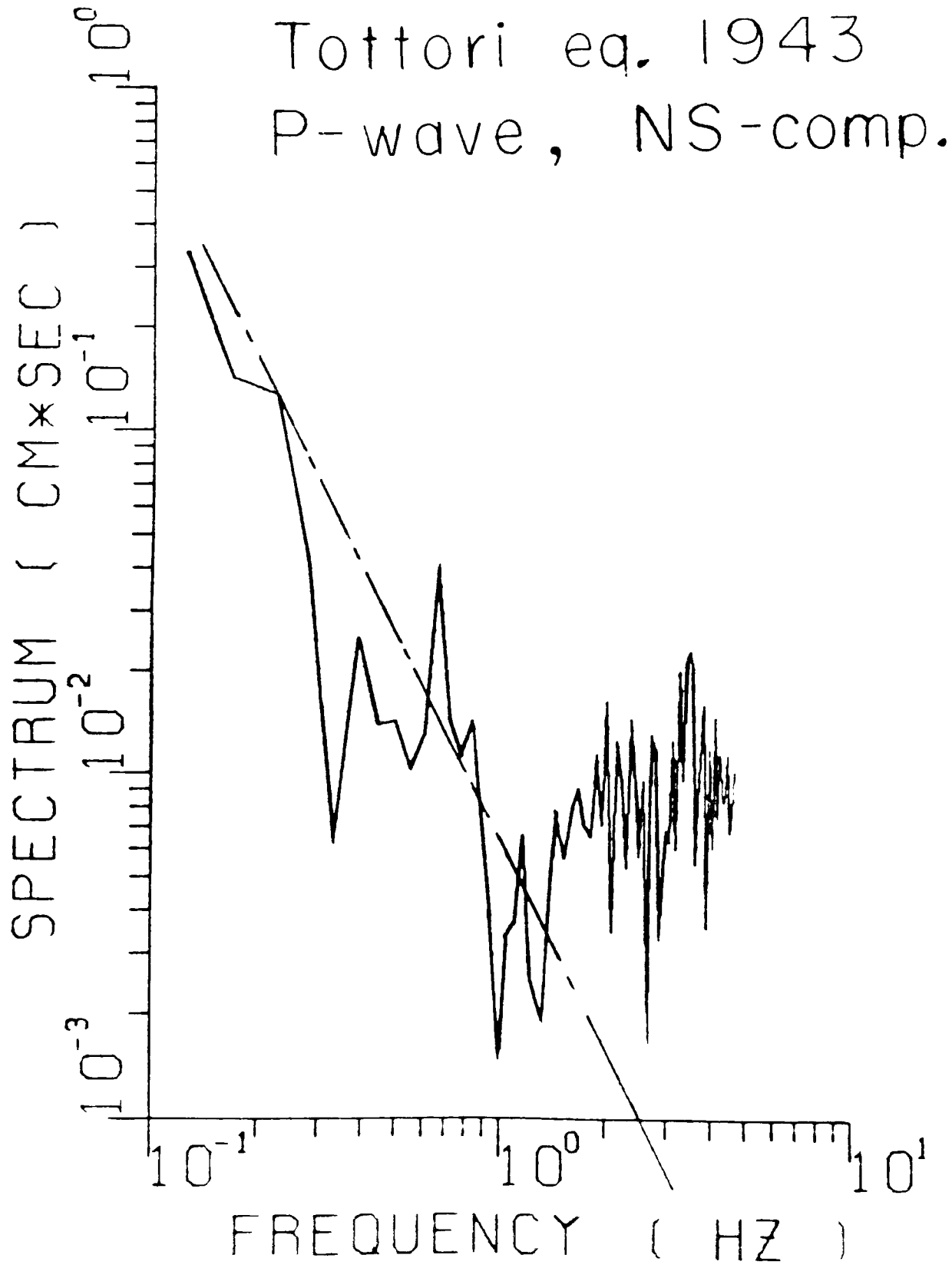
Tottori eq. 1943
P-wave, NS-comp.
SPECTRUM (CM*SEC)
10^{0}
10^{-1}
10^{-2}
10^{-3}
10^{-1}
10^{0}
10^{1}
FREQUENCY (HZ)

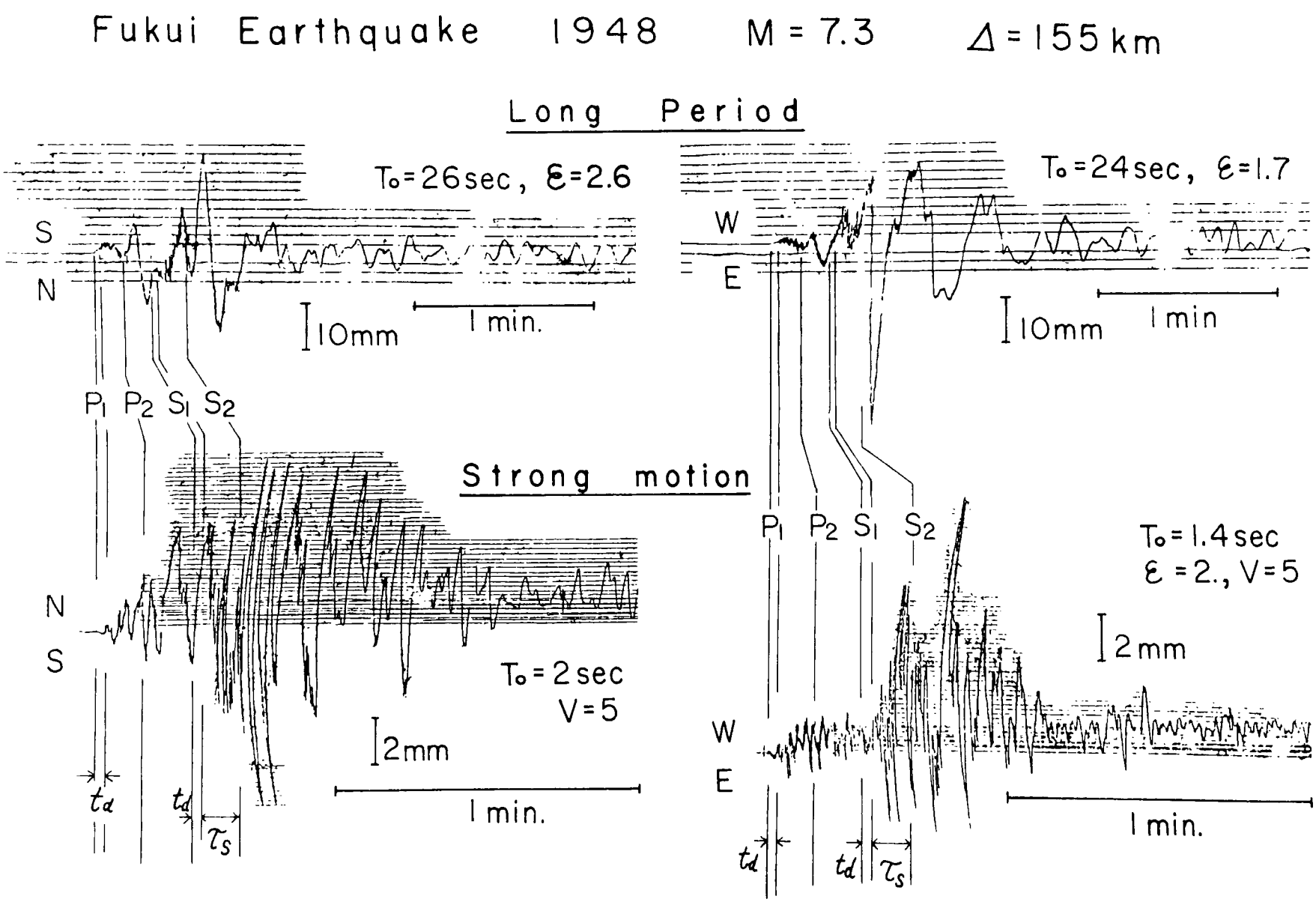
Fukui Earthquake 1948 M = 7.3 Δ = 155 km
Long Period
T₀=26sec, ε=2.6
S
N
10mm
1 min.
P₁ P₂ S₁ S₂
T₀=24sec, ε=1.7
W
E
10mm
1 min
Strong motion
N
S
T₀ = 2 sec
V=5
2mm
1 min.
P₁ P₂ S₁ S₂
T₀ = 1.4 sec
ε = 2., V=5
2mm
W
E
1 min.
t_d
t_d
τ_s
t_d
t_d
τ_s

Fig.5

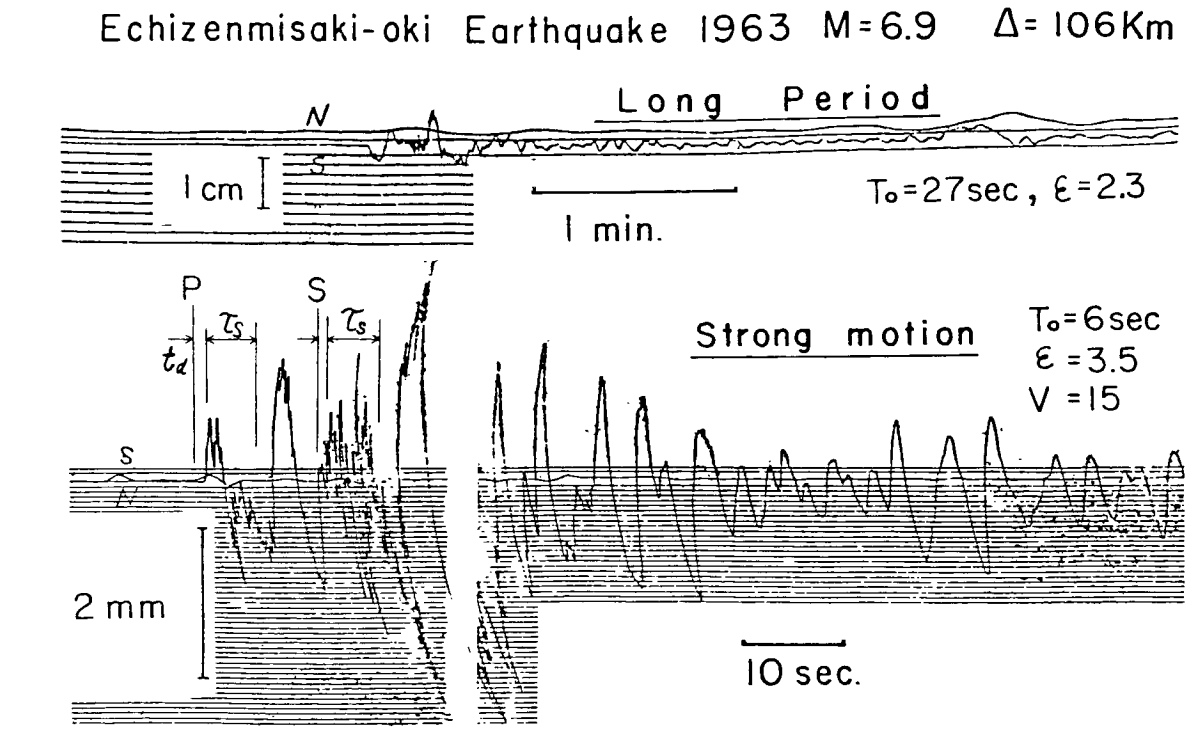
Echizenmisaki-oki Earthquake 1963 M=6.9 Δ=106Km
Long Period
N
1 cm
S
1 min.
To=27sec, ε=2.3
P
S
τs
τs
td
Strong motion
To=6sec
ε=3.5
V=15
S
2 mm
10 sec.

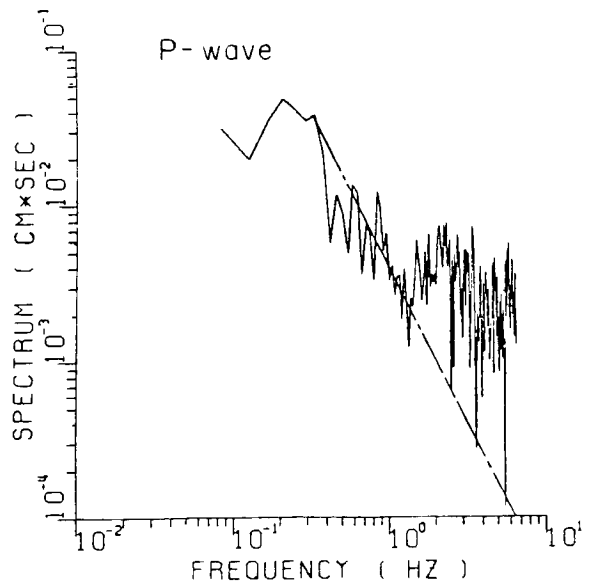
P-wave
SPECTRUM (CM×SEC)
FREQUENCY (HZ)

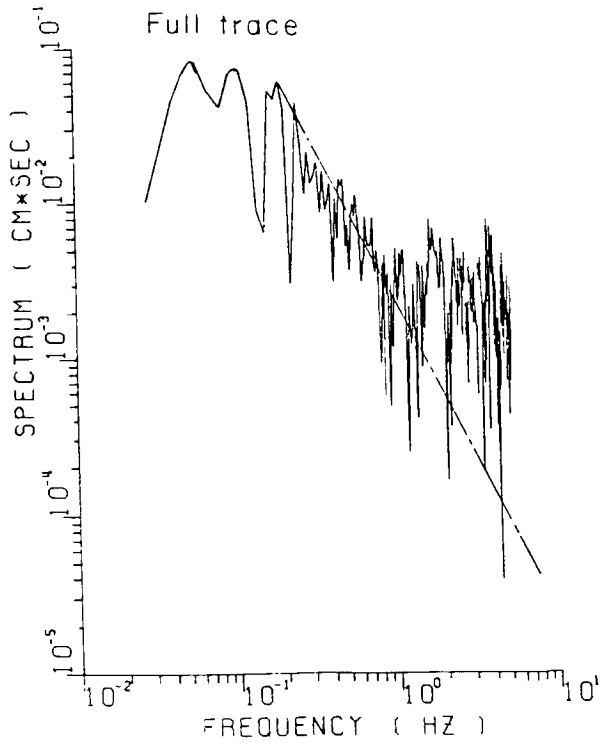
Full trace
SPECTRUM (CM×SEC)
FREQUENCY (HZ)

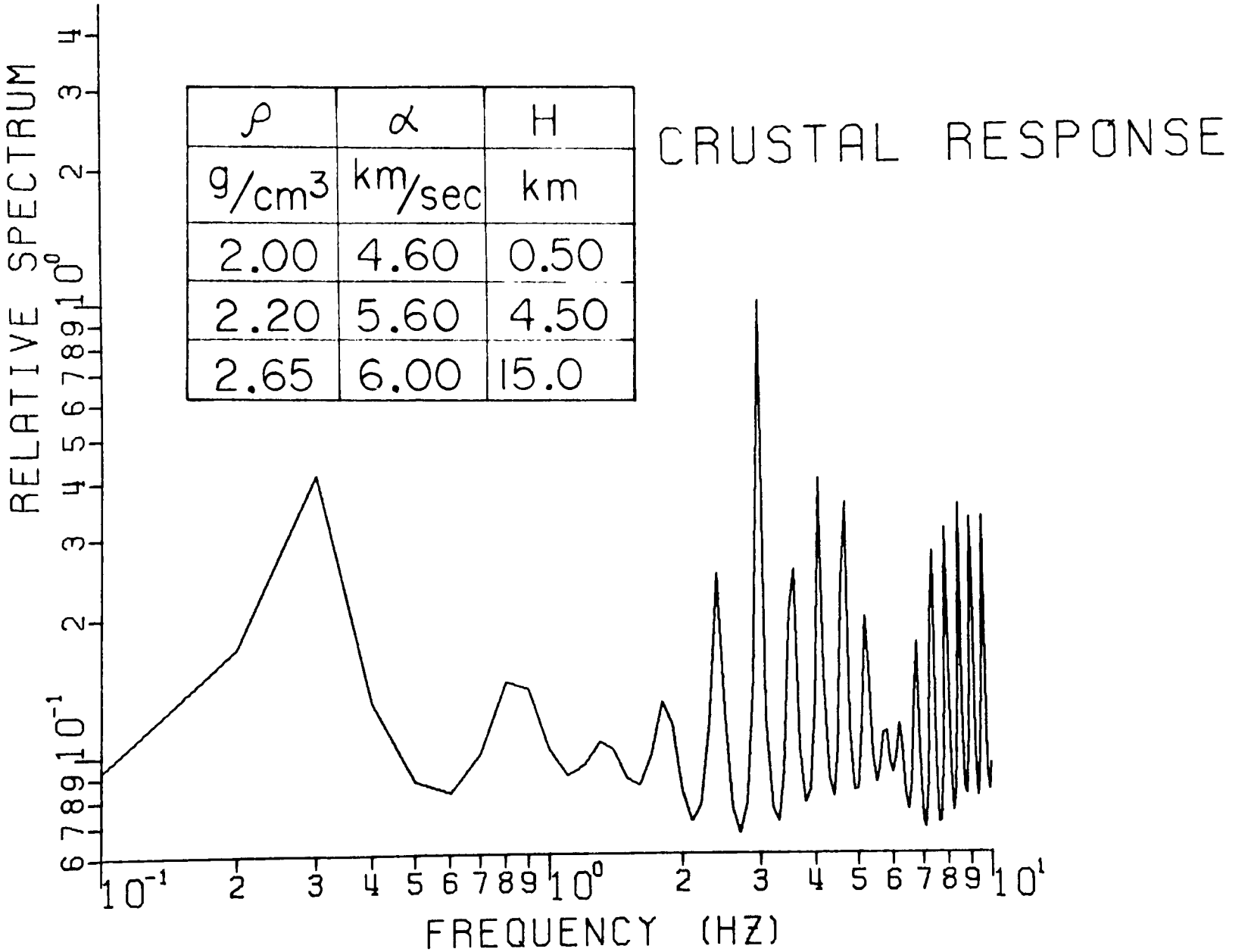

ρ	α	H
g/cm^3	km/sec	km
2.00	4.60	0.50
2.20	5.60	4.50
2.65	6.00	15.0

Fig.7

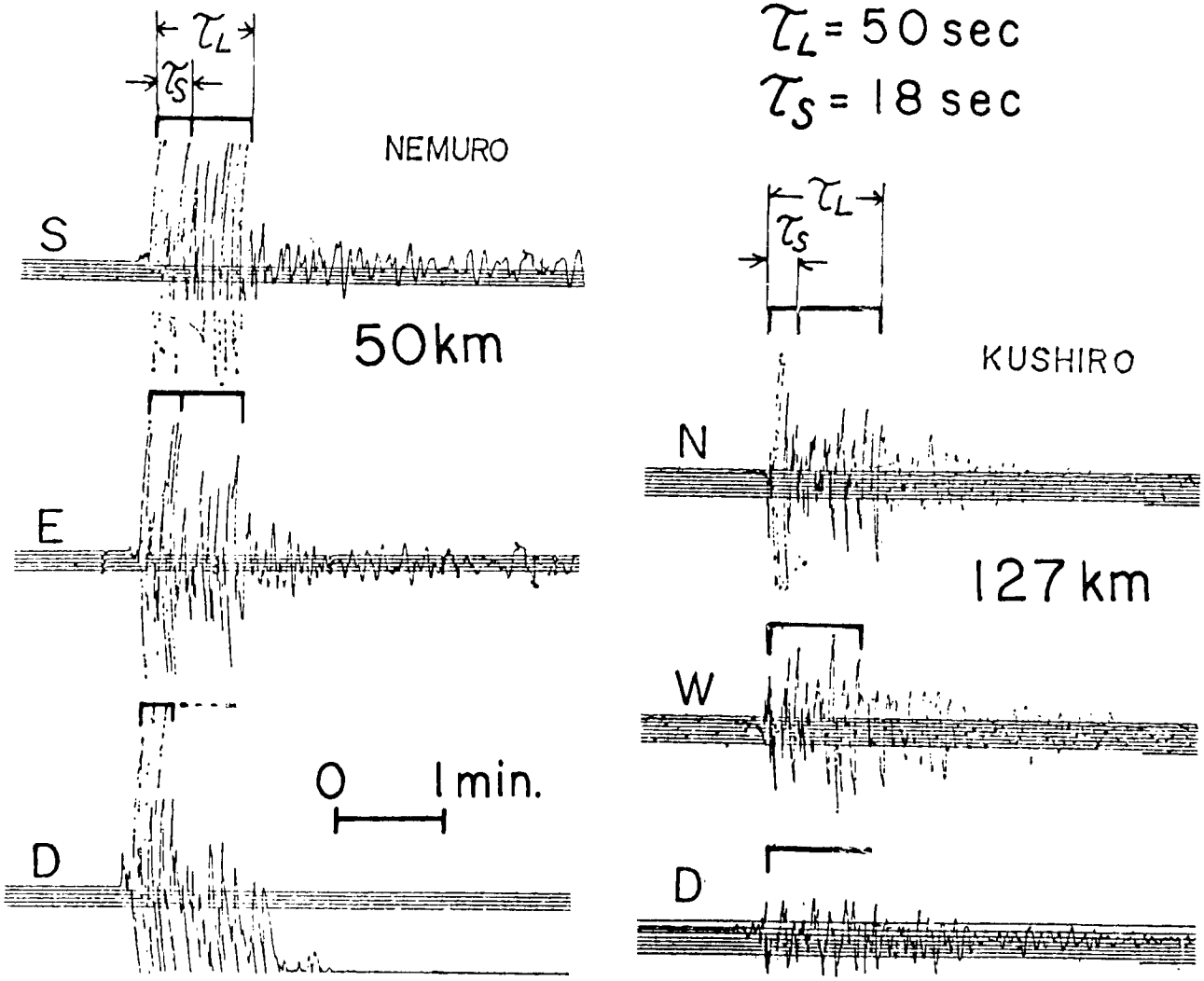
Nemuro-hanto-oki Earthquake
of June 17, 1973.
M = 7.4
τ_L = 50 sec
τ_S = 18 sec
τ_L
τ_S
NEMURO
S
50km
E
0
1 min.
D
τ_L
τ_S
KUSHIRO
N
127 km
W
D

Fig.8a

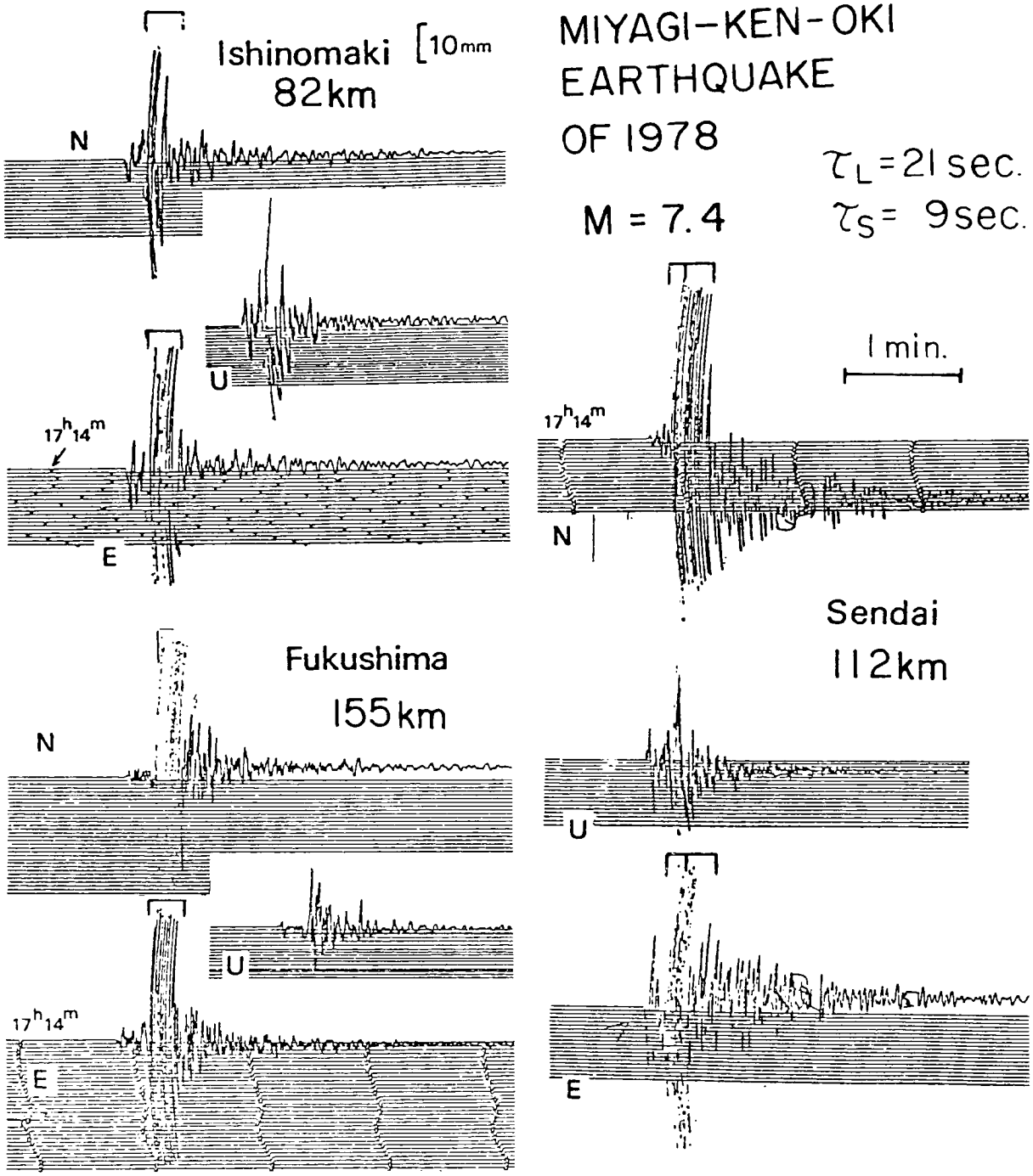
MIYAGI-KEN-OKI
EARTHQUAKE
OF 1978
M = 7.4
τ_L = 21 sec.
τ_S = 9 sec.
1 min.
Ishinomaki
82km
10mm
N
U
E
17^h14^m
Fukushima
155km
Sendai
112km

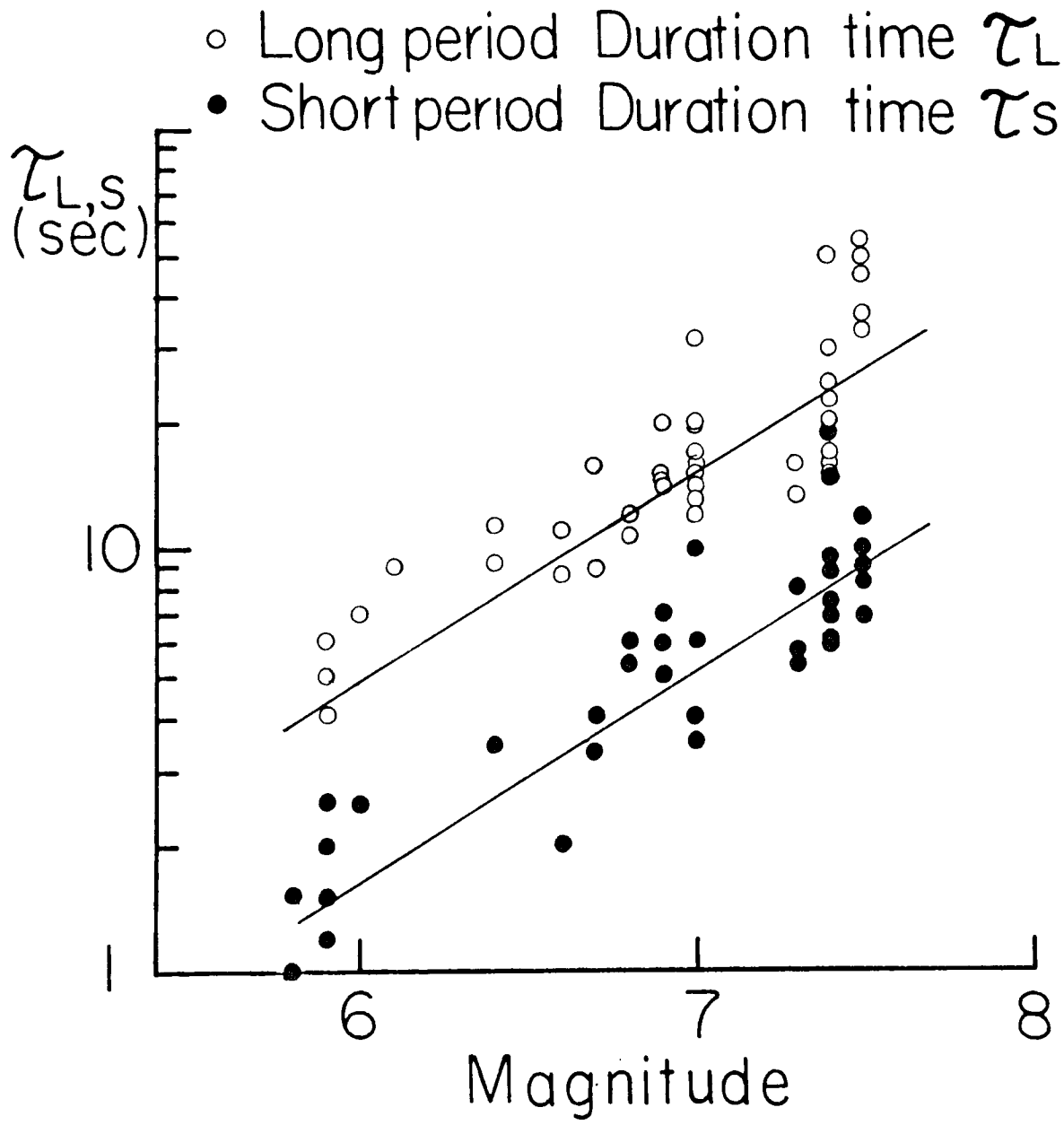
○ Long period Duration time τ_L
● Short period Duration time τ_s
$\tau_{L,S}$ (sec)
10
1
6
7
8
Magnitude

Fig.9

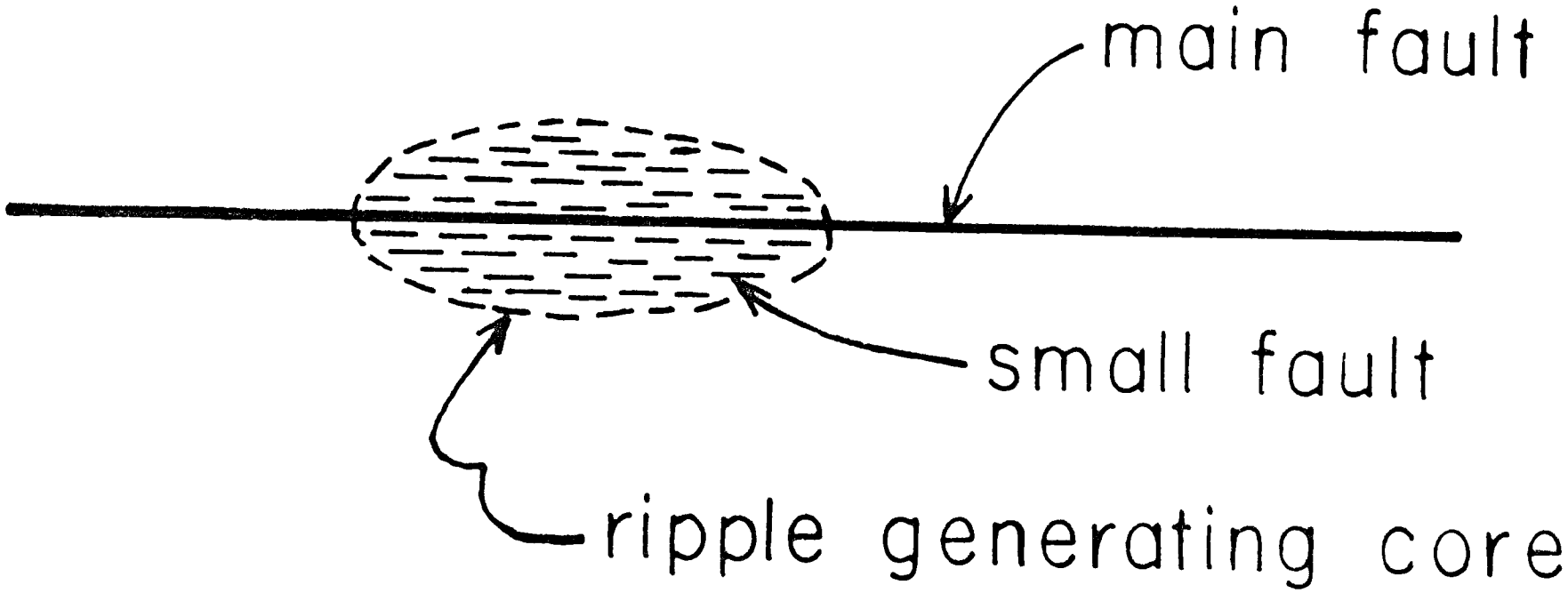

Fig.10

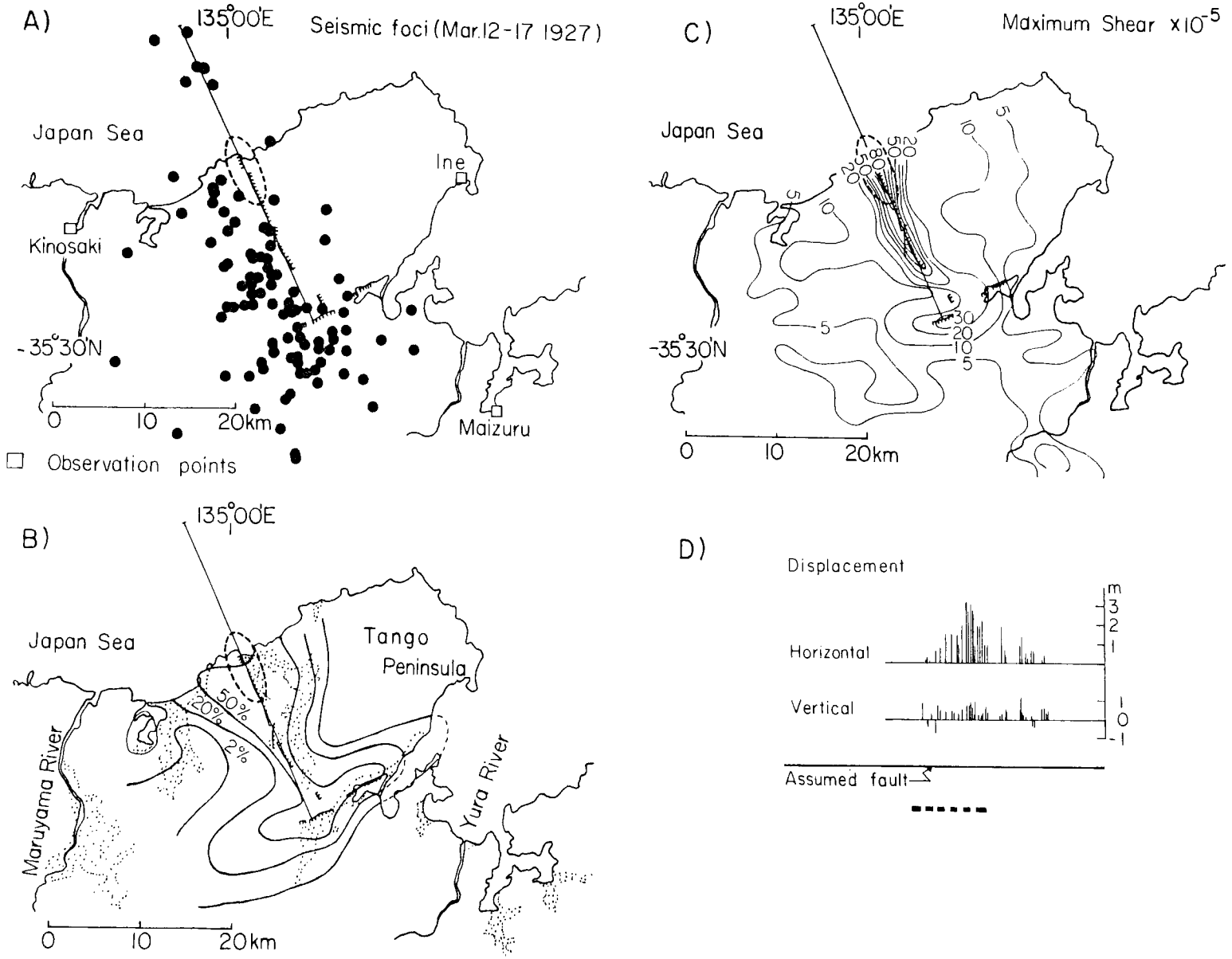
A)
135°00'E
Seismic foci (Mar.12-17 1927)
Japan Sea
Ine
Kinosaki
35°30'N
0
10
20km
Maizuru
Observation points
B)
135°00'E
Japan Sea
Tango
Peninsula
50%
20%
2%
Maruyama River
Yura River
0
10
20km
C)
135°00'E
Maximum Shear x10⁻⁵
Japan Sea
35°30'N
0
10
20km
D)
Displacement
Horizontal
Vertical
m
3
2
1
0
-1
Assumed fault

Fig.11

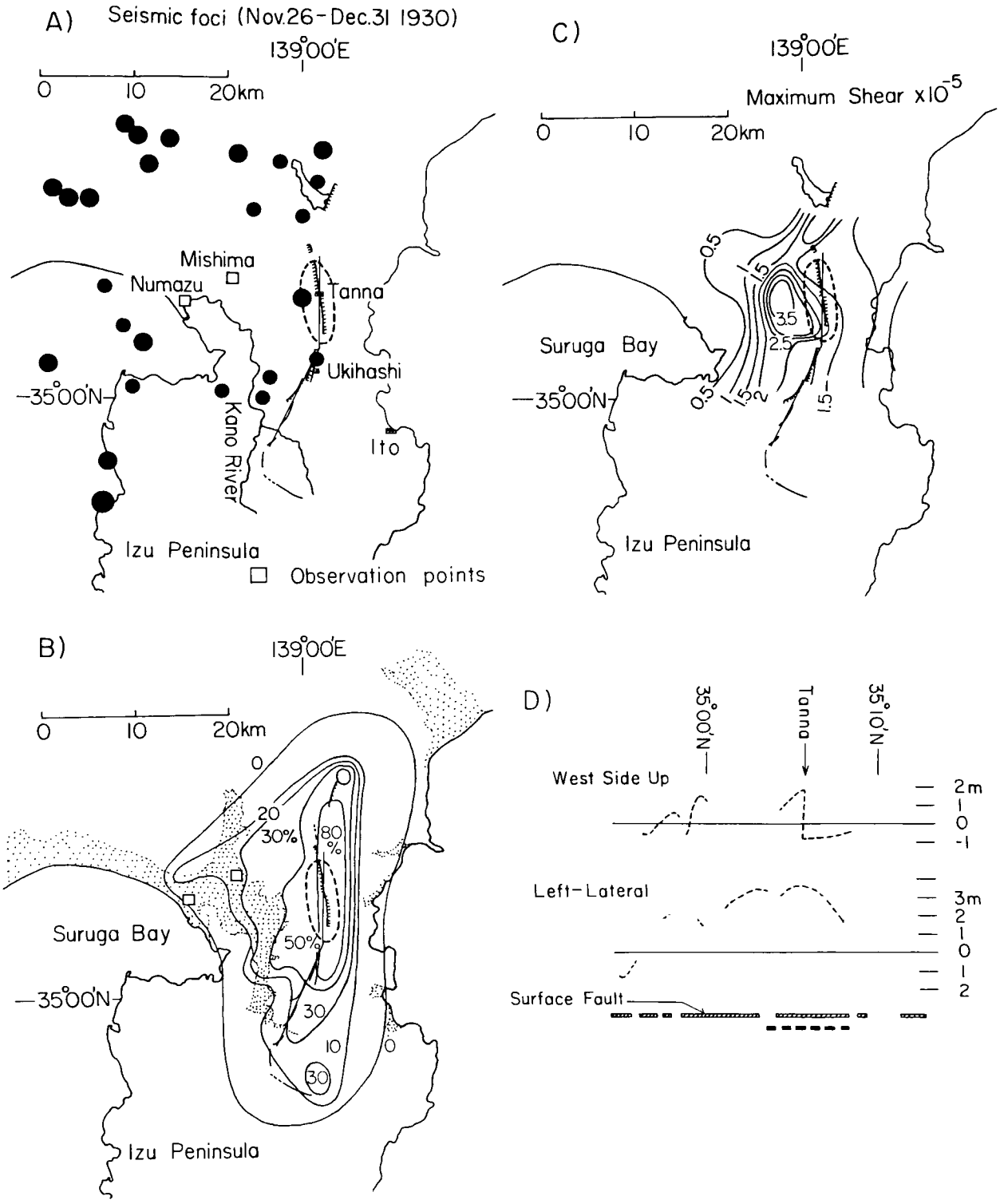
A) Seismic foci (Nov.26-Dec.31 1930)
139°00'E
0 10 20km
Mishima
Numazu
Tanna
Ukihashi
35°00'N
Kano River
Ito
Izu Peninsula
Observation points
C)
139°00'E
Maximum Shear x10⁻⁵
0 10 20km
0.5
1.5
3.5
2.5
Suruga Bay
35°00'N
Izu Peninsula
B)
139°00'E
0 10 20km
0
20
30%
80%
50%
30
10
Suruga Bay
35°00'N
Izu Peninsula
D)
35°00'N
Tanna
35°10'N
West Side Up
2m
1
0
-1
Left-Lateral
3m
2
1
0
1
2
Surface Fault

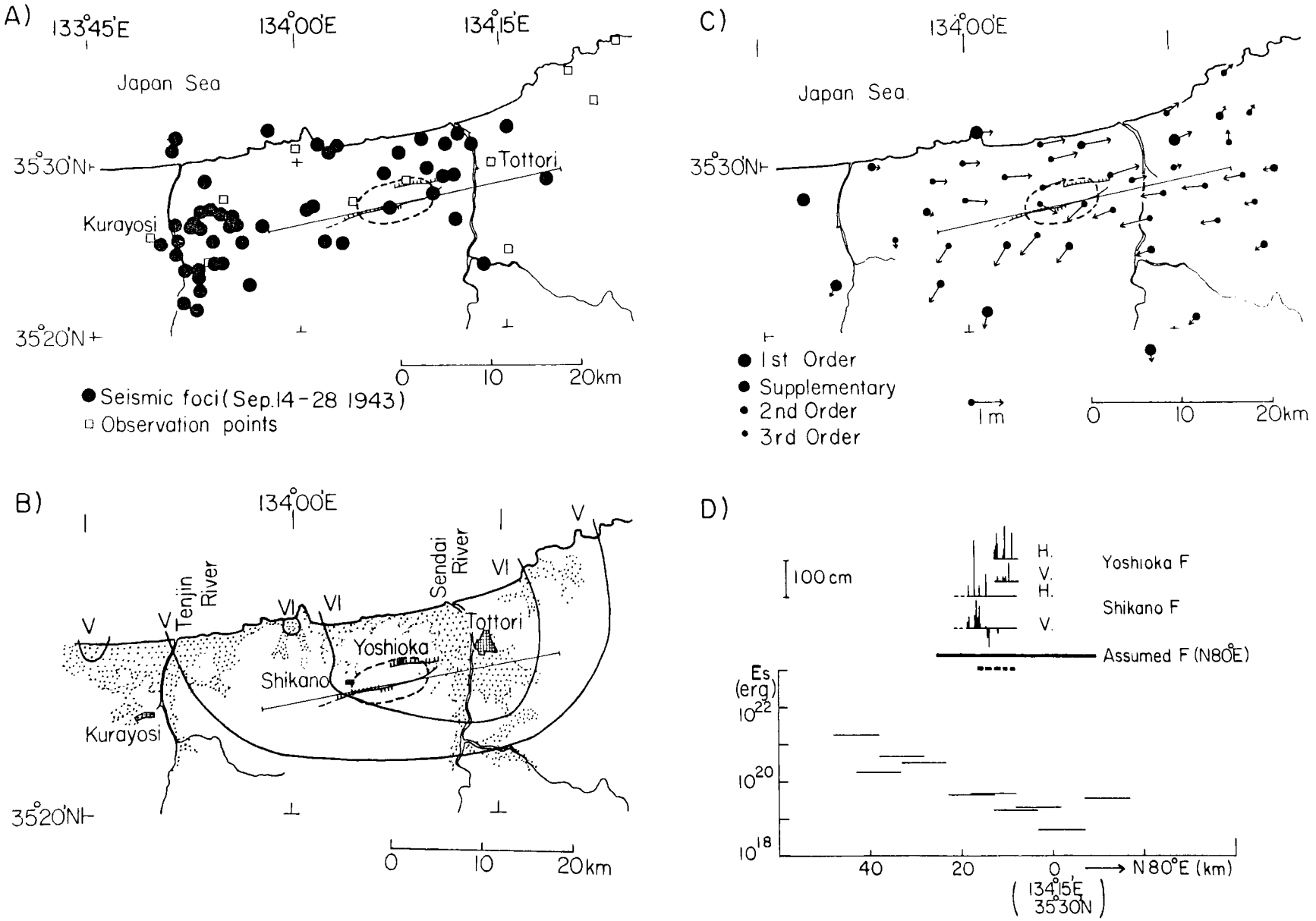
A)
133°45'E
134°00'E
134°15'E
Japan Sea
35°30'N
35°20'N
Kurayosi
Tottori
0
10
20km
Seismic foci (Sep.14-28 1943)
Observation points
B)
134°00'E
V
VI
Tenjin River
Sendai River
Yoshioka
Shikano
Tottori
Kurayosi
35°20'N
0
10
20km
C)
134°00'E
Japan Sea
35°30'N
1st Order
Supplementary
2nd Order
3rd Order
1m
0
10
20km
D)
100 cm
H.
V.
H.
V.
Yoshioka F
Shikano F
Assumed F (N80°E)
Es (erg)
10^{22}
10^{20}
10^{18}
40
20
0
N80°E (km)
(134°15'E 35°30'N)

Fig.13

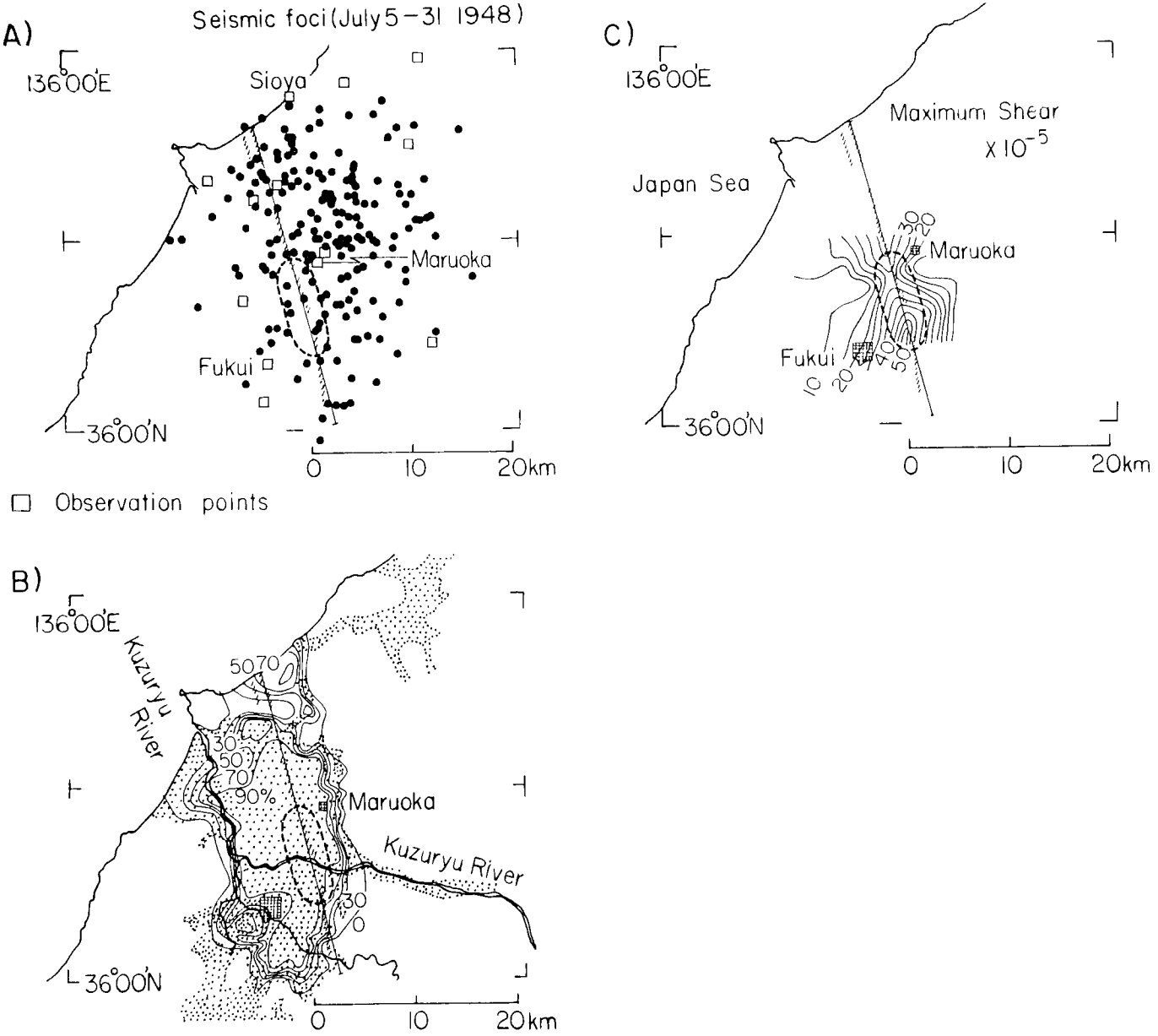
A)
Seismic foci (July 5 – 31 1948)
136°00'E
Sioya
Maruoka
Fukui
36°00'N
0
10
20km
Observation points
C)
136°00'E
Maximum Shear
X 10⁻⁵
Japan Sea
Maruoka
Fukui
36°00'N
0
10
20km
B)
136°00'E
Kuzuryu River
Maruoka
Kuzuryu River
36°00'N
0
10
20km

Fig.14

Fig.15

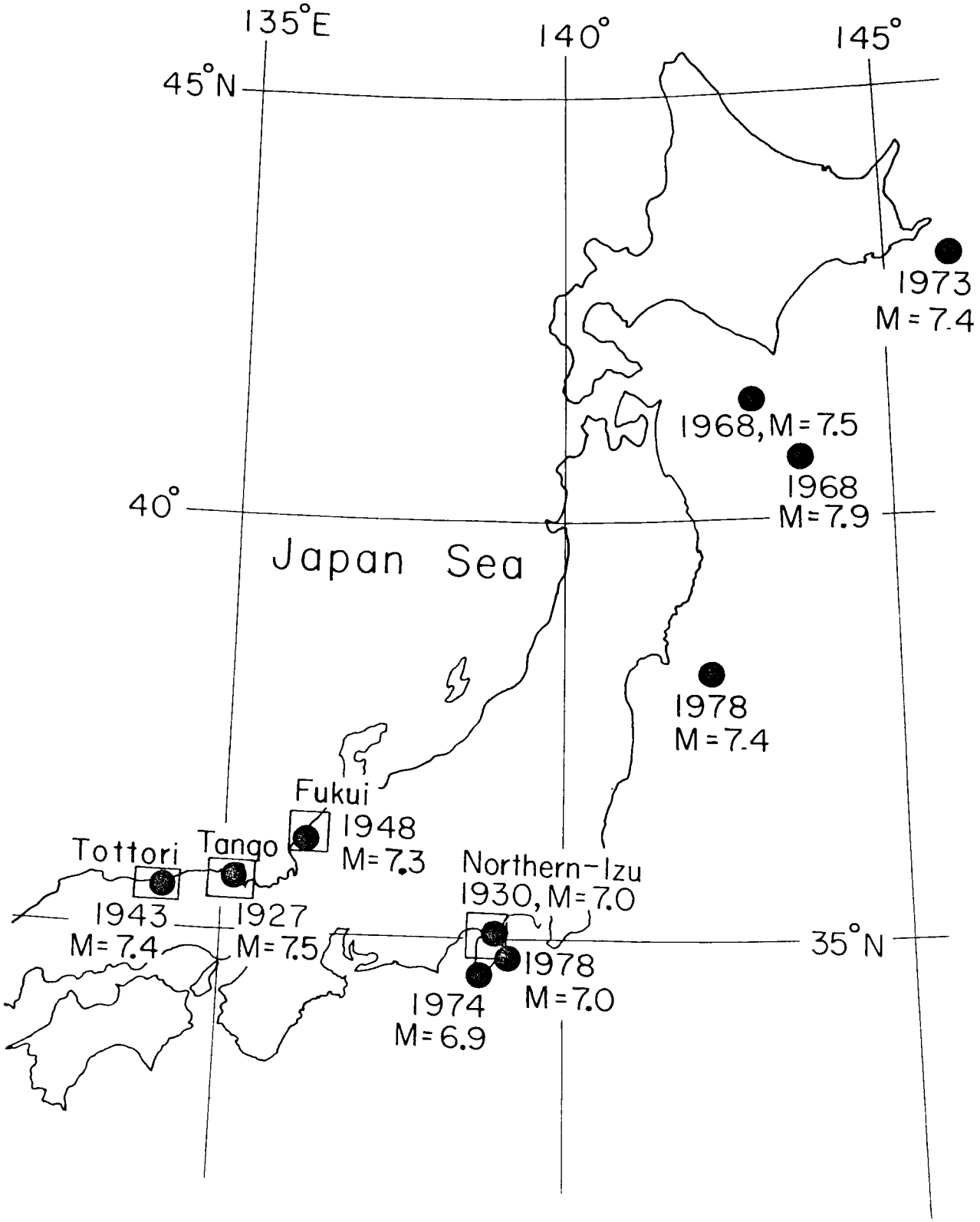
135°E
140°
145°
45°N
40°
35°N
1973
M=7.4
1968, M=7.5
1968
M=7.9
Japan Sea
1978
M=7.4
Fukui
1948
M=7.3
Tottori
Tango
1943
M=7.4
1927
M=7.5
Northern-Izu
1930, M=7.0
1978
M=7.0
1974
M=6.9

	L ℓ (km)	W w (km)	D d (m)	V v (km/sec)	T τ (sec)
L Fault	33	13	2.5	2.3	3.0
S·Fault	1	1	0.1	3.4	0.1

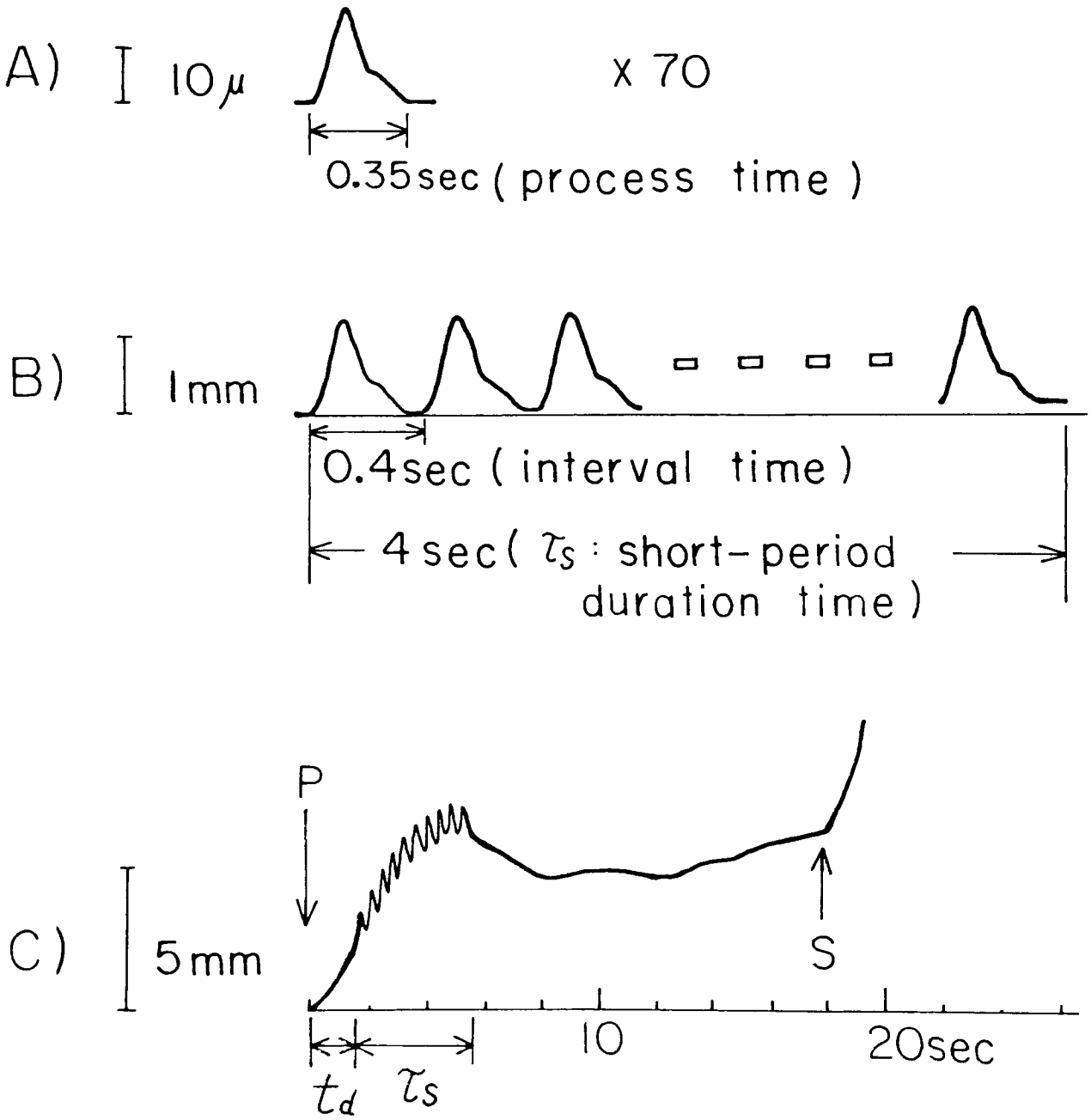

Fig.17

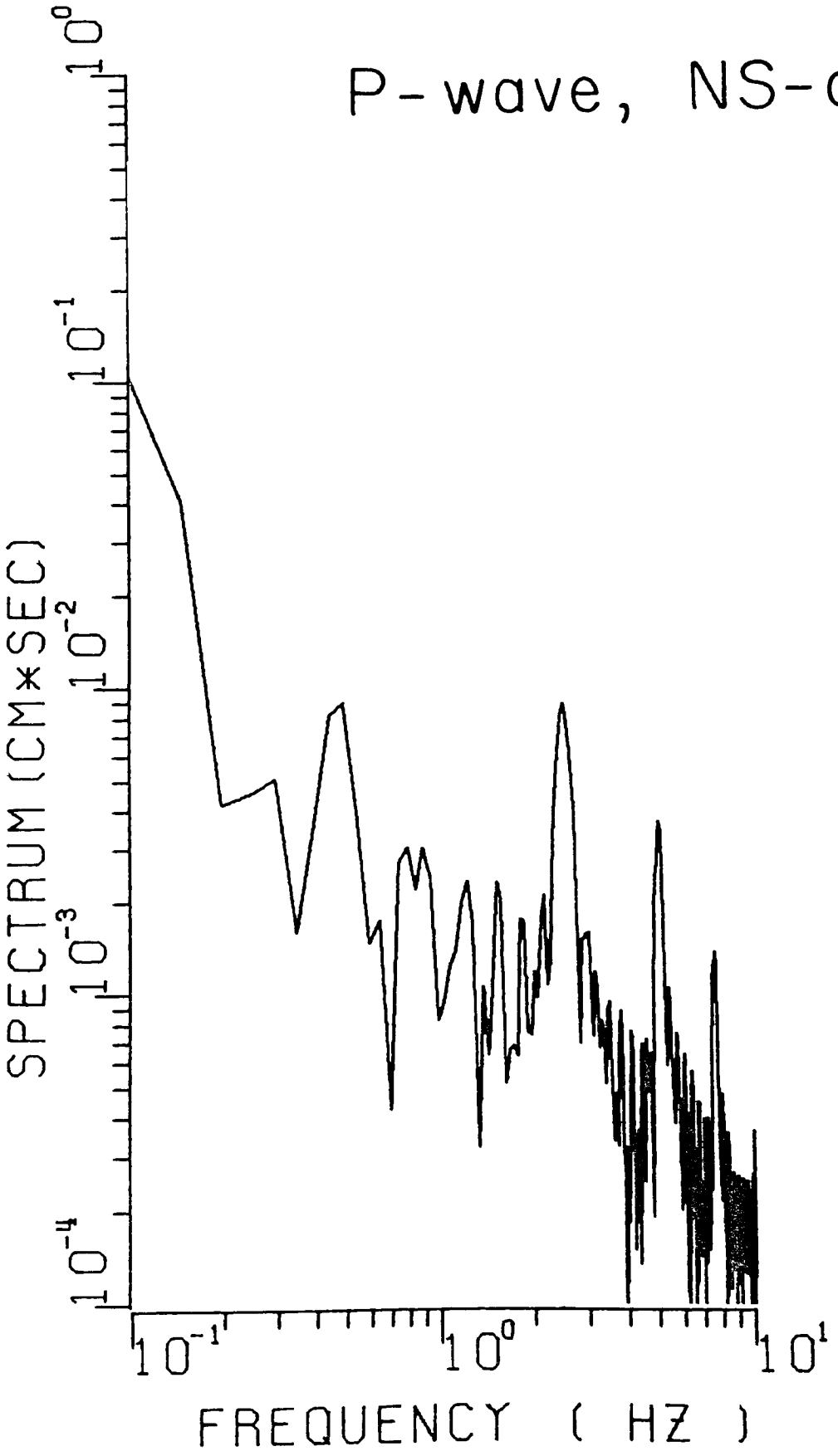
P-wave, NS-comp.
SPECTRUM (CM*SEC)
10^{0}
10^{-1}
10^{-2}
10^{-3}
10^{-4}
10^{-1}
10^{0}
10^{1}
FREQUENCY (HZ)

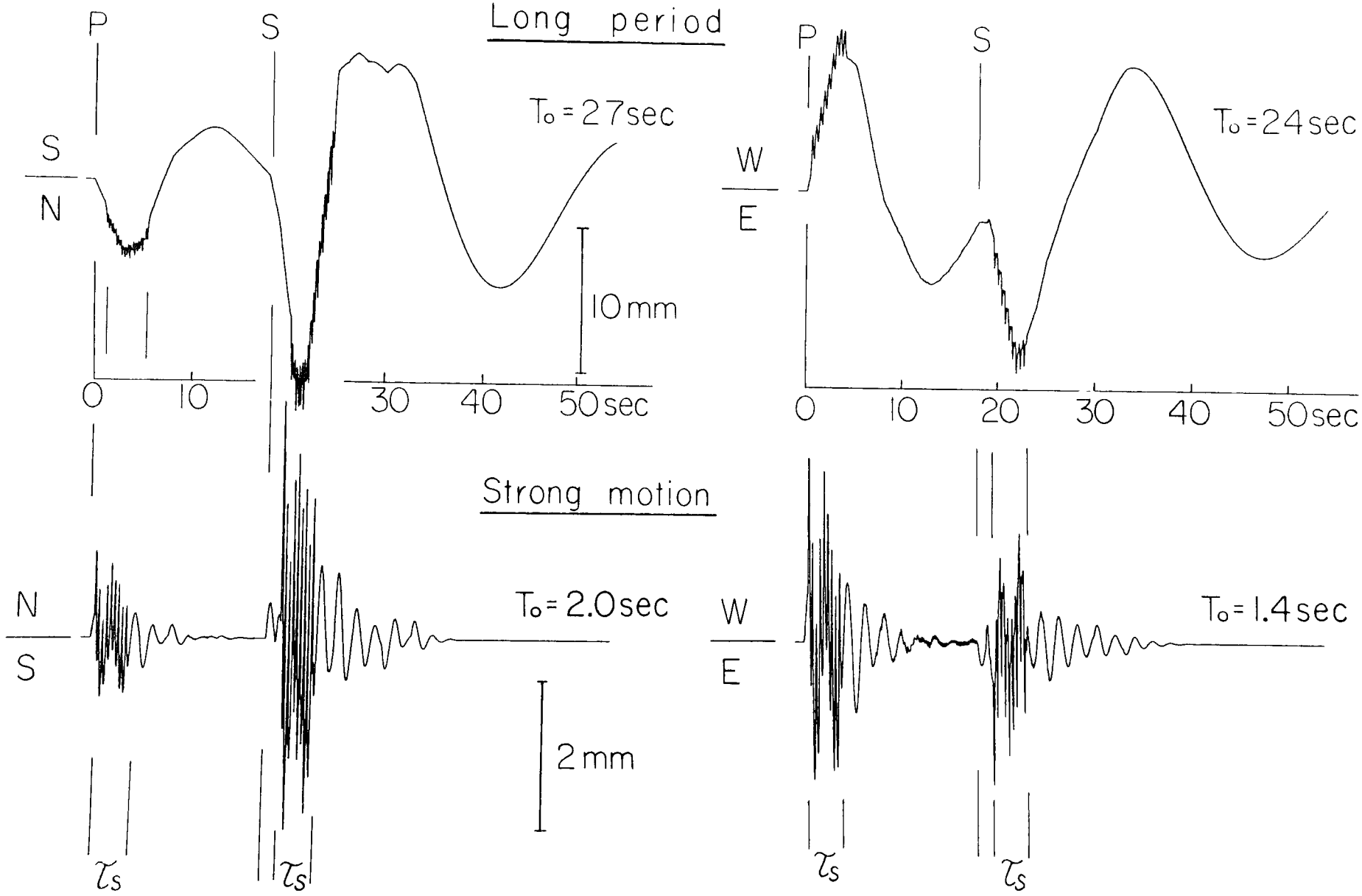
Long period
P
S
S
N
T_0 = 27sec
10mm
0
10
30
40
50sec
P
S
W
E
T_0 = 24sec
0
10
20
30
40
50sec
Strong motion
N
S
T_0 = 2.0sec
2mm
τ_s
τ_s
W
E
T_0 = 1.4sec
τ_s
τ_s

Fig.18

MIYAGI-KEN-OKI EARTHQUAKE OF 1978

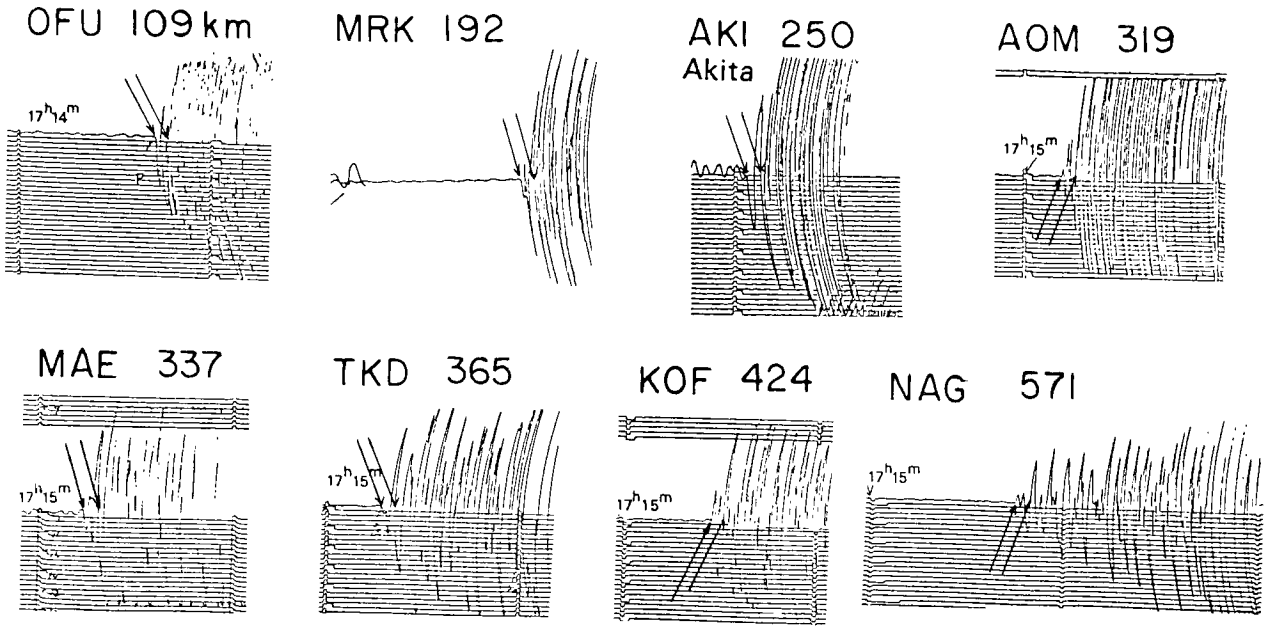

NEMURO-HANTO-OKI EARTHQUAKE OF JUNE 17, 1973

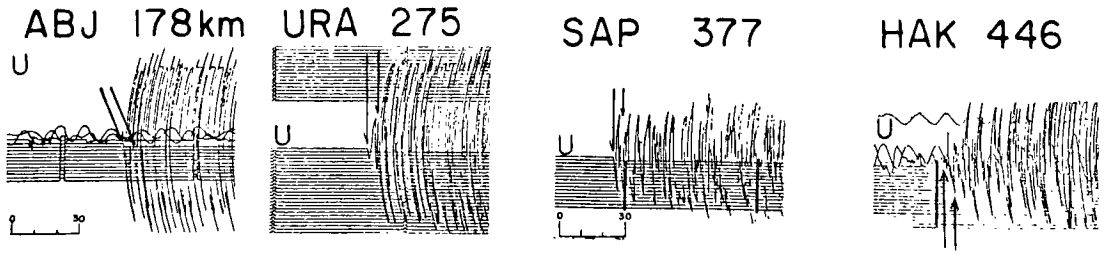

Fig.19

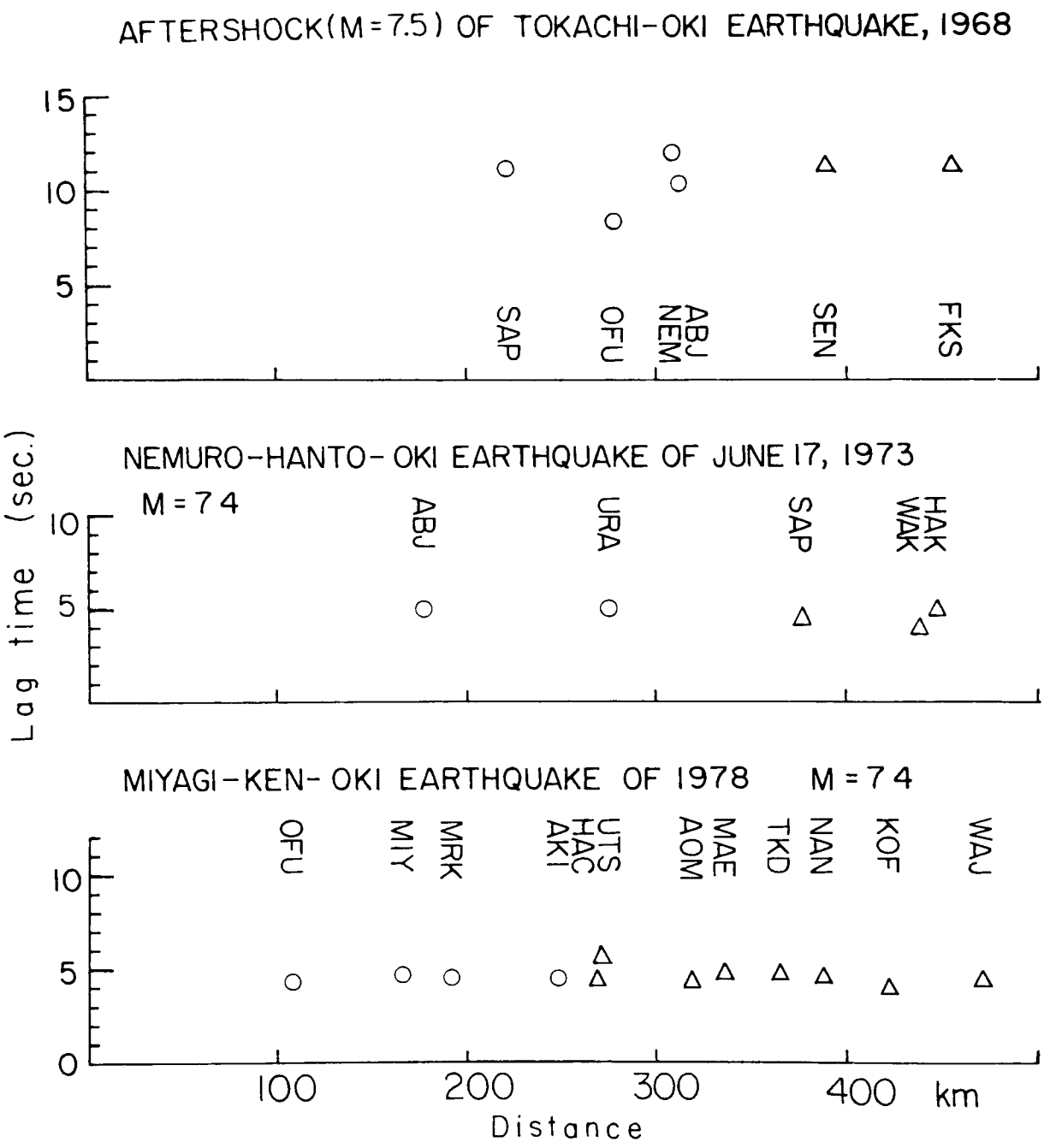
AFTERSHOCK(M=7.5) OF TOKACHI-OKI EARTHQUAKE, 1968
15
10
5
SAP
OFU
ABJ
NEM
SEN
FKS
NEMURO-HANTO-OKI EARTHQUAKE OF JUNE 17, 1973
M=7.4
Lag time (sec.)
10
5
ABJ
URA
SAP
HAK
WAK
MIYAGI-KEN-OKI EARTHQUAKE OF 1978 M=7.4
10
5
0
OFU
MIY
MRK
UTS
HAC
AKI
MAE
AOM
TKD
NAN
KOF
WAJ
100
200
300
400
km
Distance

Fig.21

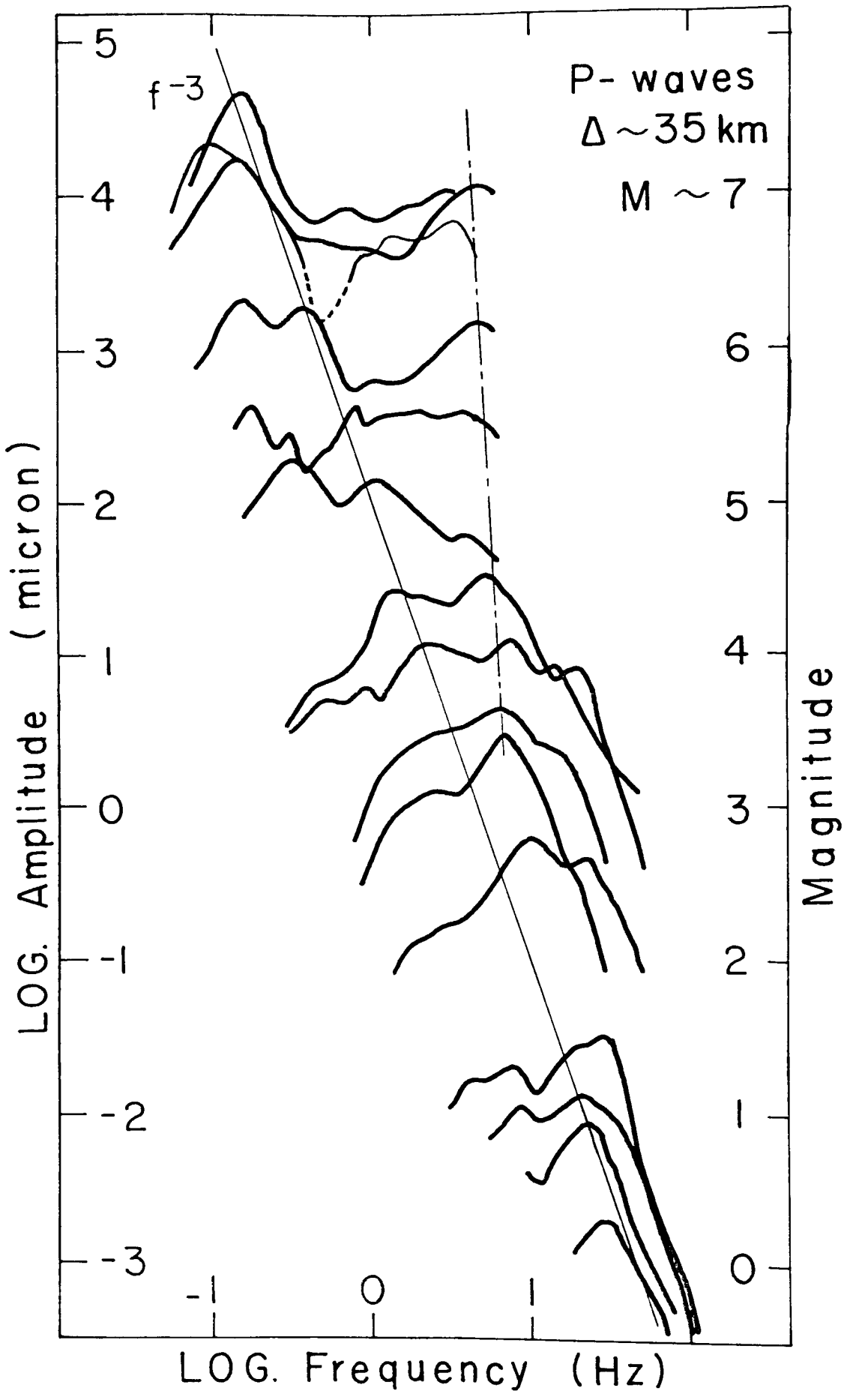
f -3
P- waves
Δ ~35 km
M ~7
LOG. Amplitude (micron)
Magnitude
LOG. Frequency (Hz)
5
4
3
2
1
0
-1
-2
-3
6
5
4
3
2
1
0
-1
0
1